NATIONAL ADVISORY COMMITTEE FOR AERONAUTICS

TECHNICAL NOTE 2702

AN APPROXIMATE METHOD OF DETERMINING THE SUBSONIC FLOW IN AN ARBITRARY STREAM FILAMENT OF REVOLUTION CUT BY ARBITRARY TURBOMACHINE BLADES

By Chung-Hua Wu, Curtis A. Brown, and Vasily D. Prian

Lewis Flight Propulsion Laboratory
Cleveland, Ohio

Washington
June 1952

1B

NATIONAL ADVISORY COMMITTEE FOR AERONAUTICS

TECHNICAL NOTE 2702

AN APPROXIMATE METHOD OF DETERMINING THE SUBSONIC FLOW IN AN ARBITRARY STREAM FILAMENT OF REVOLUTION CUT BY ARBITRARY TURBOMACHINE BLADES

By Chung-Hua Wu, Curtis A. Brown, and Vasily D. Prian

SUMMARY

A method is presented to obtain a relatively quick approximate determination of the detailed subsonic flow of a nonviscous fluid past arbitrary turbomachine blades. The governing equations are formulated as though the flow were constrained to stream filaments of revolution (the thicknesses of which vary as they pass through the machine). Attention is first fixed on a certain streamline lying between the blades and in such a filament. The shape of this streamline and the specific mass flow (product of density and velocity) along it could be estimated, for example, from the shape and the width of the channel formed by two adjacent blades and from the inlet conditions. From these starting values, the governing equations yield separate values of density and velocity components and their derivatives in the circumferential direction. These values are incorporated in a Taylor's series to provide the analytical continuation of the flow quantities from the chosen streamline to the blade surfaces. Considerations of integrated mass flow then show how the assumed shape of and specific mass flow along the chosen streamline must be adjusted to provide a starting point in a second cycle of computation.

The method is illustrated with examples of compressible flow in a turbine cascade and in a centrifugal compressor. For these high-solidity blades, three terms of the Taylor's series are found to give sufficient accuracy. Sufficient convergence is obtained in the turbine cascade after two cycles of computation (started with an available incompressible mean streamline) and in the centrifugal compressor after four cycles of computation (without any aid of available information). The detailed flow variation obtained compares very well with an available numerical solution and experimental data for the turbine cascade and with detailed experimental measurements for the centrifugal compressor. Because each cycle of computation for compressible flow takes only 16 hours, successive improvement of the solution is practical.

INTRODUCTION

A basic aerodynamic problem of gas-turbine engines is the flow of air or gas through the compressor or turbine bladings. When the distance between hub and casing is relatively short, the air or gas may be assumed, for an approximate solution, to flow along surfaces of revolution which are usually noncylindrical (figs. 1 and 2). The equations governing the flow of a nonviscous compressible fluid along such surfaces have been formulated recently by the use of a set of orthogonal coordinates l and φ (meridional and angular, respectively) on the surface (figs. 1 and 2), and general methods of solution for both subsonic and supersonic flow are given (references 1 and 2). In the case of supersonic flow, solution by the use of the method of characteristics is satisfactory. But in the case of subsonic flow, the general numerical method suggested takes a long time to accomplish if a high-speed large-scale digital computing machine is unavailable. In such a case, a much quicker approximate method of solution which gives sufficient accuracy is desirable.

When the distance between hub and casing of the compressor or turbine is relatively large, the two-dimensional solution of the flow along the surfaces of revolution cut by the blade sections becomes inadequate. A general theory of three-dimensional flow is given in reference 3, in which the complete three-dimensional flow in a turbomachine is obtained by a suitable combination of two-dimensional flows along two kinds of stream surface extending, respectively, from hub to casing and from blade to blade (fig. 3). In the first stage of such calculations, it is desirable to have some general approximate knowledge of the detailed flow variation from blade to blade obtainable by relatively quick approximate methods by assuming that the gas flows along surfaces of revolution.

For these purposes, a quick approximate method of solution of the detailed subsonic flow of a nonviscous fluid past arbitrary turbomachine blade sections along an arbitrary surface of revolution has been developed at the NACA Lewis laboratory. The method is essentially an extension of the general two-dimensional blade design method reported in reference 4 and is particularly useful for high-solidity blades, such as those encountered in axial-flow turbines and radial- or mixed-flow compressors and turbines. The method is presented and is then illustrated by two examples, namely, compressible flow past a turbine cascade and compressible flow along a curved stream filament of revolution (at the mean blade height) in a centrifugal compressor. The velocity and pressure distributions along the blade surfaces as well as across the channel are compared with available numerical solutions or experimental measurements or both.

SYMBOLS

The following symbols are used in this report:

h	static enthalpy
I	$h + \frac{1}{2} W^2 - \frac{1}{2} \omega^2 r^2$
L	blade length projected on turbomachine axis
l,φ	orthogonal coordinates on mean surface of revolution
M	mass flow
N	number of blades
P	pitch or spacing
p	static pressure of gas
p_t	total pressure of gas
r	radial distance from axis of turbomachine
T	normal channel distance from hub to casing in meridional plane
t	blade thickness in circumferential direction
U	blade speed, ωr
V	absolute velocity of gas
W	velocity of gas relative to blade
y	distance equal to $r\varphi$ for flow on cylindrical surface
z	distance along axis of turbomachine
β	slope of streamline on stream surface, $\tan^{-1} \frac{W_y}{W_z}$ or $\tan^{-1} \frac{W_\varphi}{W_l}$
γ	ratio of specific heats
Δ	correction in specific mass flow
ρ	density of gas
σ	slope of meridional curve, $\tan^{-1} \frac{W_r}{W_z}$

τ normal thickness of stream filament of revolution

ψ stream function

ω angular velocity of blade

Subscripts:

c on chosen streamline

i at inlet

l, φ meridional and circumferential components, respectively

m on mean streamline

p pressure surface of blade

s suction surface of blade

t total or stagnation state

y y-component

z z-component

Superscript:

* dimensionless value obtained by dividing by inlet value

METHOD

Equations Governing Flow on Arbitrary Surface of Revolution

When the gas is assumed to be nonviscous and to flow steadily along surfaces of revolution in turbomachines, a relatively simple description formulated in reference 1 of the governing equations for the gas flow is applicable. For the gas flowing in an arbitrary stream filament of revolution defined by the meridional coordinate l and the angular coordinate φ of the mean surface of revolution and by the varying normal thickness τ of the stream filament (fig. 1), the continuity equation takes the following form:

$$\frac{\partial(\tau\rho W_l r)}{\partial l} + \frac{\partial(\tau\rho W_\varphi)}{\partial \varphi} = 0 \qquad (1)$$

The circumferential component of the equation of motion for irrotational absolute flow is

$$\frac{\partial W_\varphi}{\partial l} - \frac{1}{r}\frac{\partial W_l}{\partial \varphi} + \left(\frac{W_\varphi}{r} + 2\omega\right) \sin \sigma = 0 \tag{2}$$

The density of the gas is related to its value at the inlet and the local gas velocity by the use of the isentropic relation between enthalpy and density of perfect gases

$$\rho^* = \frac{\rho}{\rho_i} = \left(\frac{I + \frac{1}{2}\omega^2 r^2 - \frac{1}{2}W^2}{h_i}\right)^{\frac{1}{\gamma-1}} \tag{3}$$

in which I is a constant for steady adiabatic flow.

General Description of Approximate Method of Solution

In order to obtain a relatively quick approximate solution of the flow equations (1) to (3) on a given arbitrary stream filament of revolution cut by arbitrary turbomachine blades, attention is first fixed on a particular streamline about midway between two neighboring blades (fig. 2(a)), as in the design method of reference 4. The shape of this streamline and the specific mass flow ρW_l along it are estimated from the given blade shape and the inlet and exit conditions, and separate values of velocity components and density on this chosen streamline are then easily computed. After this, successive circumferential derivatives of velocities are obtained from the values obtained on the chosen streamline, and the fluid properties in the angular direction are obtained by employing these derivatives in a Taylor's series. To this point, the calculation is exactly the same as that in the blade design method given in reference 4.

After completion of this phase of the work, the mass flow between the chosen streamline and the two given blade surfaces is computed, rather than, as in reference 4, the blade coordinates being computed for a given inlet mass flow. By comparing the relative percentages and the total mass flow with the value given at the inlet, the shape of the chosen streamline and the specific mass flow along it are corrected. In general, this process is repeated until convergence is obtained. (In the subsequent examples, after some experience on the part of the computer, the later cycles for both examples are completed within 16 hr each.) The accuracy of the solution of the problem then depends most on the number of terms used in the Taylor's series. For a check of the accuracy, the data obtained in the solution lead quickly to a calculation

of the residuals of a second-order partial differential equation in the stream function, which is obtained by combining equations (1) and (2) (see reference 4). If the residuals are found to be large, the solution can be readily improved by the relaxation technique and a more accurate solution of the given blade on the given surface is established.

Choice of Starting Streamline

The choice of the starting streamline used in the calculation depends on individual cases. In axial-flow-type machines, the streamline circumferentially dividing the mass flow in the channel into two equal parts (fig. 2(a)) is best to use and is found to resemble somewhat the blade mean line in reference 1. This streamline is designated the mean streamline, and the flow on it may be taken as the mean in the channel. In the centrifugal compressor problem to be presented later, the mean streamline is found to be too close to the suction surface of one blade. (The shape is also quite different from the blade mean line.) The extension of the flow from the mean streamline to the pressure surface of the outer blade therefore requires more terms in the series. As a compromise, a streamline having 65 percent of the mass flow between it and the suction surface of one blade is chosen.

Calculation of Flow along Chosen Streamline

If no better information is available, the shape of the chosen streamline is taken as that of the blade mean line and the specific mass flow along it is estimated as the average value between the blades according to the following relation:

$$\frac{(\rho W_l)_c \tau r}{(\rho W_l)_i \tau_i r_i} = \frac{P}{P-t} \tag{4}$$

or

$$(\rho^* W_l^*)_c = \frac{(\rho W_l)_c}{(\rho W_l)_i} = \frac{\tau_i r_i}{\tau r} \frac{P}{P-t} \tag{4a}$$

(See the appendix for the scheme of nondimensionalization.) From this value of $\rho^* W_l^*$, the slope of the chosen streamline ($\tan \beta_c$), and the given inlet condition, separate values of W_l^*, W_φ^*, and ρ^* along the chosen streamline are obtained as follows: Equation (3) is rewritten

$$\Sigma = \left(1 - \frac{\Phi}{\Sigma^2}\right)^{\frac{1}{\gamma-1}} \tag{5}$$

where

$$\Phi = (\rho^* W_l^* \sec \beta)_c^2 \frac{W_{l,i}^2}{2 h_i} \left(\frac{I + \frac{1}{2}\omega^2 r^2}{h_i}\right)^{-\frac{\gamma+1}{\gamma-1}} \tag{6}$$

and

$$\Sigma = \rho_c^* \left(\frac{I + \frac{1}{2}\omega^2 r^2}{h_i}\right)^{-\frac{1}{\gamma-1}} \tag{7}$$

Tables listing Σ in small intervals of Φ are given in reference 3 for $\gamma = 1.4$ and $4/3$. (There is a misprint of a minus sign in the exponent of equation (5) at the top of the tables given in reference 3.) With the given values of $\rho^* W_l^* \sec \beta$ along the chosen streamline, Φ is calculated according to equation (6), Σ is then read from the table, and ρ_c^* is obtained according to equation (7). After ρ_c^* is determined, $W_{l,c}^*$ and $W_{\varphi,c}$ are easily obtained by use of the following formulas:

$$W_{l,c}^* = \frac{(\rho^* W_l^*)_c}{\rho_c^*} \tag{8}$$

$$W_{\varphi,c}^* = W_{l,c}^* \tan \beta_c \tag{9}$$

Whenever there is available information concerning the flow past similar blades, this information should be used to obtain a better estimate of the shape of and the flow on the chosen streamline in the first calculation.

Angular Variation of Fluid State

The first- and second-order angular derivatives of W_l, W_φ, and ρ at the chosen streamline can be obtained from the basic equations (1), (2), and (3) (see reference 3 for derivation) as

$$\frac{\partial W_l}{\partial \varphi} = \left[r \frac{dW_\varphi}{dl} + \frac{\tan \beta}{\tau \rho} \frac{d(\tau r \rho W_l)}{dl} + (W_\varphi + 2\omega r) \sin \sigma \right] \cos^2 \beta \tag{10}$$

$$\frac{\partial W_\varphi}{\partial \varphi} = \left\{ \left[r \frac{dW_\varphi}{dl} + (W_\varphi + 2\omega r) \sin \sigma \right] \tan \beta - \frac{1}{\tau \rho} \frac{d(\tau r \rho W_l)}{dl} \right\} \cos^2 \beta \tag{11}$$

$$\frac{1}{\rho} \frac{\partial \rho}{\partial \varphi} = - \frac{1}{(\gamma - 1)\left(I + \frac{1}{2}\omega^2 r^2 - \frac{1}{2} W^2\right)} \left(W_l \frac{\partial W_l}{\partial \varphi} + W_\varphi \frac{\partial W_\varphi}{\partial \varphi} \right) \tag{12}$$

$$\frac{\partial^2 W_\varphi}{\partial \varphi^2} = \left\{ \frac{2}{\tau \rho^2} \frac{\partial \rho}{\partial \varphi} \frac{d(\tau r \rho W_l)}{dl} - \frac{1}{\tau \rho} \frac{d}{dl} \left[\tau r \left(\rho \frac{\partial W_l}{\partial \varphi} + W_l \frac{\partial \rho}{\partial \varphi} \right) \right] + \tan \beta \left(r \frac{d}{dl} \frac{dW_\varphi}{d\varphi} + \sin \sigma \frac{dW_\varphi}{d\varphi} \right) \right\} \cos^2 \beta \tag{13}$$

$$\frac{\partial^2 W_l}{\partial \varphi^2} = r \frac{d}{dl} \frac{\partial W_\varphi}{\partial \varphi} - \tan \beta \frac{\partial^2 W}{\partial \varphi^2} + \sin \sigma \frac{\partial W_\varphi}{\partial \varphi} \tag{14}$$

$$\frac{1}{\rho} \frac{\partial^2 \rho}{\partial \varphi^2} = \frac{2 - \gamma}{\rho^2} \left(\frac{\partial \rho}{\partial \varphi} \right)^2 - \frac{1}{(\gamma - 1)\left(I + \frac{1}{2}\omega^2 r^2 - \frac{1}{2} W^2\right)} \left[W_l \frac{\partial^2 W_l}{\partial \varphi^2} + W_\varphi \frac{\partial^2 W_\varphi}{\partial \varphi^2} + \left(\frac{\partial W_l}{\partial \varphi} \right)^2 + \left(\frac{\partial W_\varphi}{\partial \varphi} \right)^2 \right] \tag{15}$$

Third- and higher-order derivatives, if required, can also be obtained. The variation of any fluid property q across the channel at a constant value of l is then computed by a Taylor's series in $(\varphi - \varphi_c)$

$$q(\varphi) = q_c + (\varphi - \varphi_c) \left(\frac{\partial q}{\partial \varphi} \right)_c + \frac{(\varphi - \varphi_c)^2}{2!} \left(\frac{\partial^2 q}{\partial \varphi^2} \right)_c + \frac{(\varphi - \varphi_c)^3}{3!} \left(\frac{\partial^3 q}{\partial \varphi^3} \right)_c + \cdots \tag{16}$$

After the variation of fluid state in the angular direction is obtained, the mass flow across any constant-l line from the chosen streamline to the suction and pressure surfaces of the two adjacent blades is computed by the following formulas (fig. 4):

$$M_s = \tau r \int_{\varphi_s}^{\varphi_c} \rho W_l \, d\varphi \tag{17}$$

$$M_p = \tau r \int_{\varphi_c}^{\varphi_p} \rho W_l \, d\varphi \tag{18}$$

Correction of Shape of and Specific Mass Flow along Chosen Streamline

The correctness of the solution within the accuracy of the finite terms retained in the series is indicated by the following three items: (1) the closeness of the sum of M_s and M_p to the given inlet value, (2) the constancy of the relative magnitudes of M_s and M_p along the streamline, and (3) the closeness of the ratio of W_φ to W_l computed at the blade surface and the slope of the given blade surface.

A simple method of correction is suggested. In figure 4(a) are shown a number of stations used in obtaining the mass flow across a constant-l line, which are equally spaced in each of the two segments. The variations of ρW_l and mass flow along φ obtained in the solution are shown by the solid lines in figures 4(b) and 4(c), respectively. Whether $(M_s + M_p)$ is greater or smaller than the inlet mass flow indicates whether the ρW_l value is, in general, higher or lower, respectively, than the correct value. With the variation of ρW_l with respect to φ assumed correct, a constant (with respect to φ) Δ is added to the ρW_l values obtained in the solution to fit the mass flow; thus

$$\Delta = \frac{M_i - \tau r \int_{\varphi_s}^{\varphi_p} \rho W_l \, d\varphi}{\tau r \, (\varphi_p - \varphi_s)} \tag{19}$$

A corresponding increase in mass flow equal to $\tau r(\varphi-\varphi_s)$ multiplied by Δ is then added to the curve in figure 4(c), resulting in the dashed line. A new position of the chosen streamline φ_c' is obtained by reading from this new curve at the chosen percentage of mass flow.

This process of correction is to be applied at each station along the mean streamline. Further adjustment can be made for the right flow direction at the blade surfaces. The chosen streamline may also be corrected a short distance outside the channel by using the finite-difference equations given in reference 1, or end-point differentiation formulas may be used at the first and last stations inside the channel. If accurate determination of the velocity distribution near the leading edge is desired, either shorter spacings can be chosen there and differentiation coefficients for unequal spacings (reference 5) can be used, or a portion of the flow region near the leading edge can be improved by the finite-difference methods given in reference 1.

APPLICATIONS

The method described is applied to obtain an approximate solution of compressible flow past a turbine cascade of uniform τ and along a curved stream filament of revolution with variable τ in a centrifugal compressor.

Turbine Cascade

This is a relatively simple case of the general method. For two-dimensional flow past a cascade of blades, τ is uniform throughout and τ/τ_i is unity; also, r is a constant and $\sin \sigma = 0$. For convenience, the coordinates r and φ are combined to become y (coordinate l becomes coordinate z).

The cascade chosen is that investigated in reference 1, for which data showing detailed theoretical flow variation at inlet Mach numbers of 0.42 and 0 and the experimentally determined pressure distribution on the blade at an inlet Mach number of 0.42 are available.

The shape of the mean streamline and the variation of W_z^* obtained in the incompressible solution (see figs. 8 and 10 of reference 1) are used as the starting mean streamline and the variation of specific mass flow $\rho^* W_z^*$ along the mean streamline, respectively, for the compressible solution at an inlet Mach number of 0.42.

After the flow on the mean streamline is determined, the extension in the y-direction is accomplished by the use of the first three terms of the Taylor's series. The mass flow computed for the given blade shape is found to be somewhat high in most places and the division of mass flow is such that M_s is slightly lower than M_p. A correction is then made according to the method described. The results of the second solution are entirely satisfactory and no further correction is made. (The computation follows the setup given in reference 4.)

The starting and corrected mean streamline coordinates are shown in figure 5(a). The starting and corrected values of $(\rho^* W_z^*)_m$ and the ratio $P/(P-t)$ are shown in figure 5(b). The variation across the channel of the magnitude of the dimensionless velocity components as well as of the resultant velocity is compared with the relaxation solution of reference 4 in figure 6. The velocity distribution around the blade is compared with the relaxation solution and experimental value of reference 1 in figure 7.

In general, the comparison is satisfactory. The good correlation is especially apparent for most of the channel along the pressure surface of the blade. However, the velocity gradient of the entrance and exit sections for the suction surface of the blade is somewhat different; the experimental curve has a steeper gradient than either theoretical curve.

Flow along Curved Stream Filament of Revolution at Mean Blade Height in Centrifugal Impeller

The method is applied to a more general case of the flow along a curved surface of revolution in a centrifugal impeller for which the experimentally measured blade-to-blade flow variation at the mean blade height is available (references 6 and 7). In reference 7, the theoretical velocity distribution around the blade surface is obtained essentially by assuming that the mean streamline has the same shape as the blade mean line and that a linear variation of air velocity exists across the passage. Negative theoretical velocity, which is not observed experimentally, is obtained at the pressure surface. With the correction procedure for the shape of and the specific mass flow along the chosen streamline and the provision of a Taylor's series to consider more than a linear variation of the flow condition across the passage, the present method is applied to this impeller for a more complete comparison with the experimental data.

Simplifying assumptions. - So that this theoretical computation can be made and the results compared with the experimental data, the following assumptions must be emphasized:

(1) In order to compare the theoretical results with the available experimental data measured along the surface of revolution at the geometrical mean blade height (fig. 8), it is assumed here that the air particles lying on a circle of the mean radius 8.15 at the inlet subsequently form a stream surface of revolution which coincides with the geometrical mid-blade-height surface instrumented in the aforementioned experimental study. In general, the stream surface so formed by the

air particles lying originally on a circle at the inlet deviates from a surface of revolution. The magnitude of the deviation, however, is yet to be determined. A surface of revolution may be assumed for simplicity; if desirable, however, the position of the surface may be more accurately obtained from a hub-to-casing calculation along an S_2 surface similar to that shown in figure 3 by the method given in references 3, 8, 9, or 10. This is not done herein because experimental data are available only along the mean-blade-height surface of revolution.

(2) In the present solution, it is assumed that the ratio of the normal thickness of the stream filament τ to its inlet value is the same as the ratio of the normal distance between hub and casing T at the same place to that at the inlet; that is, τ/τ_i is equal to T/T_i. A more correct value could again be obtained from the aforementioned calculation. From the results obtained in an incompressible solution given in reference 9 for a similar centrifugal impeller, it is found that τ/τ_i is larger than T/T_i in the first half of the flow path and smaller in the second half (fig. 9). This approximation will therefore give lower and higher velocities, respectively, for these two portions.

(3) Viscosity effect is neglected in the theoretical calculation. The boundary layer in the actual flow reduces the effective channel area and thereby increases flow velocity, and the viscous losses increase the entropy of the air and reduce the rise in static pressure. These effects should be small at the inlet and increase gradually toward the exit.

Computation procedure. - Without any help of available information on the relation between the shapes of the mean streamline and the mean blade line for this type of flow (on a general surface of revolution), the starting calculation is made with an assumed mean streamline the same as the blade mean line and located midway in the channel. Its position downstream of the blade is determined on the basis of a slip factor of 0.91 and the condition that the angular momentum of the air remains constant along the streamline. The starting value of $\rho^* W_l^*$ is based on equation (4a) with an inclusion of a multiplication factor of 1.23 to account for the reduction of channel cross-sectional area caused by the taper in the blade section (see fig. 3 of reference 7). Eleven stations 1.1 inches apart are used inside the impeller (figs. 2(b) and 8). The determinations of the flow along the mean streamline and of the first and second derivatives of flow velocities in the angular direction are given in table I. The determination of the mass flow between the mean streamline and the two blade surfaces at one station is shown in table II.

The results obtained in this calculation show that the mass flows across the channel at most of the stations are lower than the given inlet value and that the division of mass flow is such that the mean streamline should be shifted considerably toward the suction surface of the blade, especially along the middle portion of the streamline. So that the location of the chosen streamline will not be too close to the suction side, a streamline which has a mass flow between it and the suction side of 65 percent of the total mass flow in the channel is used for the remaining calculations (fig. 10). The variations of $(\tau^* r^* \rho^* W_l^*)_c$ and $(\rho^* W_l^*)_c$ taken from the corrected values are shown in figures 11(a) and 11(b), respectively, by the square symbols.

With these starting values for the 65 percent streamline, a new cycle of calculation is made according to the setup shown in tables I and II. Correction in the shape of and the specific mass flow along the 65 percent streamline is further made in the same manner as previously.

The same process is repeated two more times. To expedite convergence, the corrected values obtained are not directly used as the starting value for the next cycle. Instead, an interpolated value of all previous calculations is used. This interpolation is done by plotting the starting and corrected values of each cycle of calculation along the abcissa and ordinate, respectively. The intersection of the curve joining these points and a 45° line passing through the origin is taken as the more correct value to be used as the starting value for the next cycle of calculation. The third cycle of calculation thus obtained for the 65 percent streamline shows sufficient convergence. The successive shapes of $\tau^* r^* \rho^* W_l^*$ and $\rho^* W_l^*$ for the 65 percent streamline are compared in figures 11(a) and 11(b). The accuracy of the last solution is also indicated by the values of residuals (table III) of the differential equation in the stream function computed according to the method given in reference 4. The estimated error in $\rho^* W_l^*$ divided by the approximate value is given in table IV. (These ratios indicate the order of magnitude of error in velocity.)

Comparison of theoretical and experimental flow variation. - The velocity distributions along the 10 percent and 90 percent geometrical lines taken from the experimental data reported in references 6 and 7 are compared with the theoretical value computed for the same position in figure 12. It is seen from this figure that the theoretical velocity gives a qualitative picture of the experimental variation, and that the average theoretical velocity is, in general, relatively low, especially in the first half of the flow passage. If the effect of the assumed surface of revolution for the actual twisted surface is disregarded, most of this difference probably can be attributed to the relatively large error in the assumed τ/τ_1 variation for the first half, as

indicated by figure 9. Toward the trailing edge of the blade, the reduction of flow area due to boundary layer along the blade surface should also increase the velocity in the actual case. It is of interest to note here that no negative velocity occurred at the pressure surface of the blade in the theoretical solution.

The theoretical and experimental pressures along the blade surface are compared in figure 13. In general, the two agree much better than in the case of velocity distribution, and the difference in pressure on the two sides of the blade for the experimental data is larger than that for the theoretical value. The differences among the theoretical and experimental values should be explained through the difference in velocity and the smaller increase of total pressure due to losses in the actual flow.

The theoretical and experimental variations of relative velocity and static pressure across the passage are compared in figures 14 and 15. In figure 14, the theoretical velocity is lower than the experimental value in most places. From pressure surface to suction surface, the theoretical velocity also has a higher gradient than that of an average line drawn through the experimental data. Besides the assumptions made in the theoretical calculations, there is also the experimental error in the measurements of static and total pressure; this difference in pressures is used in the computation of the experimental velocity. When the velocity is small, the normal error in the pressure measurements can cause a very large error in the velocity so computed (see reference 7).

On the other hand, the theoretical and experimental static pressures agree well throughout the passage (fig. 15). This good agreement indicates that the present approximate method of solution should be useful in predicting, comparing, or improving the performance of, at least, similar type machines.

CONCLUDING REMARKS

A method is presented to obtain a relatively quick approximate solution of the detailed subsonic flow of a nonviscous fluid past arbitrary turbomachine blades along a given arbitrary surface of revolution. The method is illustrated with examples of compressible flow in a turbine cascade and in a centrifugal compressor. Three terms in the series to account for the circumferential flow variation from the chosen streamline about midway in the channel to the blade surface are found to be sufficient. For a centrifugal compressor, the mean streamline shape is found quite different from that of the blade mean line; consequently, correction for the mean streamline shape is necessary. Sufficient convergence is obtained after two cycles of computation for the turbine

cascade and four cycles for the centrifugal compressor. (Each cycle of computation can be done in 16 hr.) The detailed flow variations obtained compared very well with an available numerical solution and experimental measurements.

Lewis Flight Propulsion Laboratory
National Advisory Committee for Aeronautics
Cleveland, Ohio, February 12, 1952

APPENDIX - NONDIMENSIONALIZATION OF EQUATIONS

In the examples, all quantities are made dimensionless as follows:

$$r^* = \frac{r}{r_i} \; ; \quad \tau^* = \frac{\tau}{\tau_i} \; ; \quad l^* = \frac{l}{r_i} \; ; \quad W_l^* = \frac{W_l}{W_{l,i}} \; ; \quad W_\varphi^* = \frac{W_\varphi}{W_{l,i}} \; ;$$

$$W^* = \frac{W}{W_{l,i}} \; ; \quad U^* = \frac{U}{W_{l,i}} \; ; \quad \rho^* = \frac{\rho}{\rho_i} \; ; \quad h^* = \frac{h}{W_{l,i}^2} \; ; \quad I^* = \frac{I}{W_{l,i}^2} \; ; \quad M^* = \frac{M}{\tau_i r_i \rho_i W_{l,i}}$$

In this dimensionless form, equations (3), (4a), (6), (7), (10) to (14), and (16) to (18) appear as follows:

$$\rho^* = \left(\frac{I^* + \frac{1}{2} U_i^{*2} r^{*2} - \frac{1}{2} W^{*2}}{h_i^*} \right)^{\frac{1}{\gamma - 1}} \tag{3'}$$

$$\left(\rho^* W_l^* \right)_c = \frac{1}{\tau^* r^*} \frac{P}{P - t} \tag{4a'}$$

$$\Phi = (\rho^* W_l^* \sec \beta)_c^2 \frac{W_{l,i}^{*2}}{2h_i^*} \left(\frac{I^* + \frac{1}{2} U_i^{*2} r^{*2}}{h_i^*} \right)^{-\frac{\gamma+1}{\gamma-1}} \tag{6'}$$

$$\Sigma = \rho_c^* \left(\frac{I^* + \frac{1}{2} U_i^{*2} r^{*2}}{h_i^*} \right)^{-\frac{1}{\gamma-1}} \tag{7'}$$

$$\frac{\partial W_l^*}{\partial \varphi} = \left[r^* \frac{dW_\varphi^*}{dl^*} + \frac{\tan \beta}{\tau^* \rho^*} \frac{d(\tau^* r^* \rho^* W_l^*)}{dl^*} + \left(W_\varphi^* + 2U_i^* r^* \right) \sin \sigma \right] \cos^2 \beta \tag{10'}$$

$$\frac{\partial W_\varphi^*}{\partial \varphi} = \left\{ \left[r^* \frac{dW_\varphi^*}{dl^*} + \left(W_\varphi^* + 2U_i^* r^* \right) \sin \sigma \right] \tan \beta - \frac{1}{\tau^* \rho^*} \frac{d(\tau^* r^* \rho^* W_l^*)}{dl^*} \right\} \cos^2 \beta \tag{11'}$$

$$\frac{1}{\rho^*} \frac{\partial \rho^*}{\partial \varphi} = - \frac{1}{(\gamma - 1)\left(I^* + \frac{1}{2} U_i^{*2} r^{*2} - \frac{1}{2} W^{*2} \right)} \left[W_l^* \frac{\partial W_l^*}{\partial \varphi} + W_\varphi^* \frac{\partial W_\varphi^*}{\partial \varphi} \right] \tag{12'}$$

$$\frac{\partial^2 W_\varphi^*}{\partial \varphi^2} = \left\{ \frac{2}{\tau^* \rho^{*2}} \frac{\partial \rho^*}{\partial \varphi} \frac{d(\tau^* r^* \rho^* W_l^*)}{dl^*} - \frac{1}{\tau^* \rho^*} \frac{d\left[\tau^* r^* \left(\rho^* \frac{\partial W_l^*}{\partial \varphi} + W_l^* \frac{\partial \rho^*}{\partial \varphi} \right) \right]}{dl^*} + \right.$$

$$\left. \tan \beta \left(r^* \frac{d}{dl^*} \frac{\partial W_\varphi^*}{\partial \varphi} + \sin \sigma \frac{\partial W_\varphi^*}{\partial \varphi} \right) \right\} \cos^2 \beta \tag{13'}$$

$$\frac{\partial^2 W_l^*}{\partial \varphi^2} = r^* \frac{d}{dl^*} \frac{\partial W_\varphi^*}{\partial \varphi} - \tan \beta \frac{\partial^2 W_\varphi^*}{\partial \varphi^2} + \sin \sigma \frac{\partial W_\varphi^*}{\partial \varphi} \tag{14'}$$

$$W_l^* = (W_l^*)_c + \left(\frac{\partial W_l^*}{\partial \varphi} \right)_c (\varphi - \varphi_c) + \frac{1}{2!} \left(\frac{\partial^2 W_l^*}{\partial \varphi^2} \right) (\varphi - \varphi_c)^2 + \ldots \tag{16'}$$

$$M_s^* = \tau^* r^* \int_{\varphi_s}^{\varphi_c} \rho^* W_l^* \, d\varphi \tag{17'}$$

$$M_p^* = \tau^* r^* \int_{\varphi_c}^{\varphi_p} \rho^* W_l^* \, d\varphi \tag{18'}$$

In the second example, the velocity and static pressure are given in terms of, respectively, the velocity of sound at the inlet total condition and the inlet total pressure

$$\frac{W}{a_{t,i}} = \frac{W_{l,i}}{a_{t,i}} W^*$$

$$\frac{p}{p_{t,i}} = \frac{p_i}{p_{t,i}} \rho^{*1.4}$$

The dimensionless form of the partial differential equation in the stream function used to compute the residual is obtained from equations (4) and (5) of reference 1 or equation (26') of reference 4. (In that equation, the last term in the second parenthesis, $2\omega\rho \sin \sigma$, should have a minus sign.)

$$\frac{\partial^2 \psi^*}{\partial l^{*2}} + \left(\frac{\sin \sigma}{r^*} - \frac{\partial \ln \tau^*}{\partial l^*} \right) \frac{\partial \psi^*}{\partial l^*} + \frac{1}{r^{*2}} \frac{\partial^2 \psi^*}{\partial \varphi^2} +$$

$$\tau^* \left(W_\varphi^* \frac{\partial \rho^*}{\partial l^*} - \frac{W_l^*}{r^*} \frac{\partial \rho^*}{\partial \varphi} - 2U_i^* \rho^* \sin \sigma \right) = 0$$

$$\frac{\partial \psi^*}{\partial \varphi} = \tau^* \rho^* W_l^* r^*$$

$$- \frac{\partial \psi^*}{\partial l^*} = \tau^* \rho^* W_\varphi^*$$

REFERENCES

1. Wu, Chung-Hua, and Brown, Curtis A.: Method of Analysis for Compressible Flow Past Arbitrary Turbomachine Blades on General Surface of Revolution. NACA TN 2407, 1951.

2. Wu, Chung-Hua, and Costilow, Eleanor L.: A Method of Solving the Direct and Inverse Problem of Supersonic Flow Along Arbitrary Stream Filaments of Revolution in Turbomachines. NACA TN 2492, 1951.

3. Wu, Chung-Hua: A General Theory of Three-Dimensional Flow in Subsonic and Supersonic Turbomachines of Axial-, Radial- and Mixed-Flow Types. NACA TN 2604, 1952.

4. Wu, Chung-Hua, and Brown, Curtis A.: A Method of Designing Turbomachine Blades with a Desirable Thickness Distribution for Compressible Flow Along an Arbitrary Stream Filament of Revolution. NACA TN 2455, 1951.

5. Wu, Chung-Hua: Formulas and Tables of Coefficients for Numerical Differentiation with Function Values Given at Unequally Spaced Points and Application to Solution of Partial Differential Equations. NACA TN 2214, 1950.

6. Michel, Donald J., Ginsburg, Ambrose, and Mizisin, John: Experimental Investigation of Flow in the Rotating Passages of a 48-Inch Impeller at Low Tip Speeds. NACA RM E51D20, 1951.

7. Prian, Vasily D., and Michel, Donald J.: An Analysis of Flow in Rotating Passage of Large Radial-Inlet Centrifugal Compressor at Tip Speed of 700 Feet per Second. NACA TN 2584, 1951.

8. Wu, Chung-Hua: A General Through-Flow Theory of Fluid Flow with Subsonic or Supersonic Velocity in Turbomachines of Arbitrary Hub and Casing Shapes. NACA TN 2302, 1951.

9. Ellis, Gaylord, Stanitz, John D., and Sheldrake, Leonard J., Jr.: Two Axial-Symmetry Solutions for Incompressible Flow Through a Centrifugal Impeller with and without Inducer Vanes. NACA TN 2464, 1951.

10. Hamrick, Joseph T., Ginsburg, Ambrose, and Osborn, Walter M.: Method of Analysis for Compressible Flow Through Mixed-Flow Centrifugal Impellers of Arbitrary Design. NACA TN 2165, 1950.

TABLE I - COMPUTATION OF FLOW ON MEAN STREAMLINE AND FIRST AND SECOND φ-DERIVATIVES AT MEAN STREAMLINE

Station	①	②	③	④	⑤	⑥	⑦	⑧	⑨	⑩
	l	r^*	τ^*	$\tau^* r^*$	φ_m	$\sin \sigma$	From curve $\left(\tau^* \rho^* r^* W_l^*\right)_m$	$\left(\rho^* W_l^*\right)_m$	$r^* \frac{\partial \varphi_m}{\partial l^*}$ tan β_m	$\sec^2 \beta_m$ ⑨^2 + 1
1	0	1	1	1	------	------	1	1	-1.1573	2.3393
2	1.1	1.0086	1.0375	1.0464	------	------	1.0018	.9574	-1.1779	2.3874
3	2.2	1.0589	1.0333	1.0942	------	0.5707	1.0100	.9230	-1.2539	2.5723
4	3.3	1.1571	.9475	1.0964	------	.7907	1.0265	.9362	-1.3771	2.8799
5	4.4	1.2736	.8580	1.0927	------	.8969	1.0600	.9701	-1.4792	3.1880
6	5.5	1.4025	.7747	1.0865	------	.9636	1.1290	1.0391	-1.5238	3.3214
7	6.6	1.5337	.7000	1.0736	-0.2599	.9788	1.2100	1.1270	-1.4500	3.1025
8	7.7	1.6663	.6229	1.0379	-.3730	.9890	1.2210	1.1764	-1.2629	2.5949
9	8.8	1.8012	.5536	.9971	-.4624	.9926	1.1747	1.1781	-1.0247	2.0500
10	9.9	1.9350	.5000	.9675	-.5274	.9945	1.1414	1.1797	-.7727	1.5971
11	11.0	2.0699	.4583	.9486	-.5708	.9962	1.1175	1.1781	-.5382	1.2897
12	12.1	2.2049	.4250	.9371	-.5983	.9976	1.0990	1.1728	-.3324	1.1105
13	13.2	2.3399	.3958	.9261	-.6139	.9985	1.0857	1.1723	-.1850	1.0342
14	14.3	2.4748	.3705	.9170	-.6201	.9986	1.0740	1.1712	-.0524	1.0027
15	15.4	2.6086	.3479	.9075	-.6209	.9987	1.0637	1.1721	0	1
16	16.5	2.7436	.3271	.8974	-.6199	.9990	1.0540	1.1745	0	1
17	17.6	2.8820	.3083	.8885	-.6204	.9992	1.0450	1.1761	-.1595	1.0254
18	18.7	3.0135	.2917	.8790	------	.9993	1.0360	1.1766	-.4347	1.1890
19	19.8	3.1497	.2759	.8690	------	.9994	1.0277	1.1826	-.7573	1.5735
20	20.9	3.2834	.2622	.8610	------	.9997	1.0193	1.1839	-1.0490	2.1004
21	22.0	3.4200	.2500	.8550	------	.9997	1.0119	1.1835	-1.3312	2.7721
22	23.1	3.5521	.2400	.8525	------	------	1.0056	1.1796	-1.5865	3.5170
23	24.2	3.6883	.2333	.8605	------	------	1	1.1621	-1.8547	4.4399

TABLE I - COMPUTATION OF FLOW ON MEAN STREAMLINE AND FIRST AND SECOND φ-DERIVATIVES AT MEAN STREAMLINE - Continued

Station	(11) $(\rho^* W_l^* \sec\beta)_m^2$ (8)^2 (10)	(12) $\frac{I^* + \frac{1}{2}U_1^{*2} r^{*2}}{h_1^*}$ 0.01127 (2)^2 $+1.0084$	(13) $\left(\frac{I^* + \frac{1}{2}U_1^{*2} r^{*2}}{h_1^*}\right)^{\frac{1}{\gamma-1}}$ (12)$^{2.5}$	(14) $\left(\frac{I^* + \frac{1}{2}U_1^{*2} r^{*2}}{h_1^*}\right)^{-\frac{\gamma+1}{\gamma-1}}$ (12)$^{-6}$	(15) $5\,\Phi$ $5\,\frac{W_{l,i}^2}{2h_i}$ (11) (14)	(16) Σ from table	(17) ρ_m^* (13) (16)	(18) $W_{l,m}^*$ (8) / (17)	(19) $W_{\varphi,m}^*$ (9) (18)
1	2.3393	1.0197	1.0500	0.8895	0.0875	0.9525	1.0001	0.9999	-1.1572
2	2.1883	1.0199	1.0505	.8885	.0815	.9560	1.0043	.9533	-1.1229
3	2.1914	1.0210	1.0533	.8828	.0813	.9561	1.0071	.9165	-1.1492
4	2.5241	1.0235	1.0598	.8699	.0920	.9498	1.0066	.9301	-1.2755
5	3.0002	1.0267	1.0681	.8538	.1075	.9403	1.0043	.9659	-1.4288
6	3.5862	1.0306	1.0783	.8346	.1255	.9288	1.0016	1.0374	-1.5808
7	3.9406	1.0349	1.0895	.8140	.1345	.9229	1.0055	1.1208	-1.6252
8	3.5911	1.0397	1.1022	.7917	.1195	.9327	1.0280	1.1444	-1.4453
9	2.8452	1.0450	1.1163	.7679	.0920	.9498	1.0602	1.1112	-1.1386
10	2.2227	1.0508	1.1313	.7437	.0695	.9629	1.0894	1.0829	-.8368
11	1.7900	1.0567	1.1478	.7183	.0540	.9716	1.1153	1.0583	-.5685
12	1.5274	1.0632	1.1656	.6923	.0445	.9768	1.1385	1.0301	-.3424
13	1.4215	1.0701	1.1846	.6660	.0400	.9793	1.1600	1.0106	-.1870
14	1.3754	1.0774	1.2049	.6393	.0370	.9809	1.1819	.9909	-.0519
15	1.3738	1.0851	1.2265	.6126	.0355	.9817	1.2040	.9735	0
16	1.3795	1.0932	1.2495	.5859	.0340	.9825	1.2277	.9567	0
17	1.4183	1.1018	1.2743	.5590	.0335	.9827	1.2522	.9392	-.1497
18	1.8516	1.1107	1.3001	.5326	.0370	.9809	1.2752	.9242	-.4017
19	2.2006	1.1202	1.3281	.5061	.0470	.9755	1.2955	.9129	-.6913
20	2.9440	1.1299	1.3571	.4806	.0585	.9686	1.3144	.9007	-.9448
21	3.8828	1.1400	1.3876	.4556	.0745	.9601	1.3323	.8883	-1.1825
22	4.8938	1.1506	1.4201	.4310	.0885	.9519	1.3518	.8728	-1.3844
23	5.9960	1.1617	1.4546	.4069	.1025	.9434	1.3723	.8468	-1.5706

TABLE I - COMPUTATION OF FLOW ON MEAN STREAMLINE AND FIRST AND SECOND φ-DERIVATIVES AT MEAN STREAMLINE - Continued

Station	(20) $r^* \frac{dW^*_\varphi}{dl^*}$ ② $\frac{d(19)}{dl^*}$	(21) $\frac{1}{\tau^*\rho^*_m}$ $\frac{1}{③\ ⑰}$	(22) $\frac{d(\tau^* r^* \rho^* W^*_l)_m}{dl^*}$ $\frac{d(7)}{dl^*}$	(23) $\left(W^*_\varphi + 2U^*_1 r^*\right)_m \sin\sigma$ $(2.3168\ ② + ⑲) \times ⑥$	(24) $\cos^2\beta_m$ $\frac{1}{⑩}$	(25) $\frac{1}{\tau^*\rho^*_m}\frac{d(\tau^* r^* \rho^* W^*_l)_m}{dl^*}$ ㉑ ㉒	(26) $\left(\frac{\partial W^*_l}{\partial\varphi}\right)_m$ $\left(⑨\ ㉕ + ⑳ + ㉓\ ㉔\right)$	(27) $\left(\frac{\partial W^*_\varphi}{\partial\varphi}\right)_m$ $\frac{⑳ + ㉓ - ㉖}{⑨}$
1	-------	------	------	------	0.4275	------	------	-------
2	-------	------	------	------	.4189	------	------	-------
3	-0.6195	0.9610	0.0850	0.7442	.3888	0.0817	0.0087	-0.0925
4	-1.2710	1.0485	.1684	1.1113	.3472	.1766	-.1395	.0147
5	-1.5463	1.1605	.3828	1.3650	.3137	.4442	-.2630	-.0552
6	-1.2133	1.2888	.6208	1.6080	.3011	.8001	-.2482	-.4220
7	1.7502	1.4208	.3856	1.8892	.3223	.5450	.5960	-1.4092
8	3.2397	1.5617	-.1820	2.3886	.3854	-.2842	2.3075	-2.6295
9	4.2386	1.7038	-.3361	3.0120	.4878	-.5726	3.8231	-3.3449
10	4.1312	1.8359	-.2072	3.6261	.6261	-.3804	5.0409	-3.5155
11	3.8386	1.9564	-.1545	4.2109	.7754	-.3023	6.3677	-3.1249
12	3.0863	2.0667	-.1155	4.7545	.9005	-.2387	7.1321	-2.1321
13	2.5362	2.1780	-.0903	5.2262	.9669	-.1967	7.5407	-1.1984
14	1.7627	2.2836	-.0809	5.6738	.9973	-.1847	7.4261	-.1985
15	.6087	2.3874	-.0737	6.0357	1	-.1760	6.6444	0
16	-1.4361	2.4902	-.0689	6.3500	1	-.1716	4.9139	0
17	-4.4882	2.5903	-.0667	6.5220	.9752	-.1728	2.0102	-.1480
18	-6.3037	2.6883	-.0640	6.5754	.8410	-.1721	.2914	.0453
19	-6.4408	2.7978	-.0621	6.6020	.6355	-.1737	.1860	.0327
20	-5.9741	2.9016	-.0593	6.6605	.4761	-.1721	.4127	-.2609
21	-5.5693	3.0023	-.0506	6.7389	.3607	-.1519	.4948	-.5069
22	-------	------	------	------	.2843	------	------	-------
23	-------	------	------	------	.2252	------	------	-------

NACA

TABLE I - COMPUTATION OF FLOW ON MEAN STREAMLINE AND FIRST AND SECOND φ-DERIVATIVES AT MEAN STREAMLINE - Concluded

Station	(28) $\frac{1}{2} W_m^{*2} \left((18)^2 + (19)^2\right) \times 0.5$	(29) $\frac{h_i}{W_{z_i}^2}$ (12) - (28) 59.5238 (12) - (28)	(30) (18)(26) + (19)(27)	(31) $\frac{1}{\rho_m^*} \frac{\partial \rho_m^*}{\partial \varphi}$ 2 (31)(25) $- \frac{2.5\,(30)}{(29)}$	(32)	(33) (18)(31) + (26)	(34) (4)(17)(33)	(35) $\frac{d(34)}{dz^*}$	(36) $\frac{d(27)}{dz^*}$	(37) (2)(36) + (8)(27)	(38) $\left(\frac{\partial^2 W_\varphi^*}{\partial \varphi^{*2}}\right)_m$ [- (21)(35) + (32) + (37)(8)] X (24)	(39) $\left(\frac{\partial^2 W_z^*}{\partial \varphi^2}\right)_m$ -(9)(38) + (37)
1	1.1695	59.5269	------	------	-------	------	------	-------	------	-------	-------	-------
2	1.0848	59.6235	------	------	-------	------	------	-------	------	-------	-------	-------
3	1.0803	59.6935	0.1145	-0.0048	-0.00078	0.0043	0.0047	-------	------	-------	-------	-------
4	1.2457	59.6769	-.1485	.0062	.0022	-.1337	-.1476	-------	------	-------	-------	-------
5	1.4872	59.6259	-.1752	.0073	.0065	-.2559	-.2808	-1.0026	-1.3440	-1.7612	1.1843	-0.0084
6	1.7872	59.5580	.4085	-.0172	-.0275	-.2660	-.2895	2.4140	-5.0553	-7.4967	2.4941	-3.6967
7	1.9487	59.6525	2.9582	-.1240	-.1352	.4570	.4933	9.5485	-8.8725	-14.9885	2.5886	-11.2350
8	1.6993	60.1876	6.4411	-.2675	.1520	2.0014	2.1354	12.3890	-7.6511	-15.3496	.0729	-15.2575
9	1.2656	60.9368	8.0567	-.3305	.3785	3.4558	3.6532	10.1544	-3.3170	-9.2947	-3.6089	-12.9827
10	.9385	61.5992	8.4008	-.3409	.2594	4.8717	4.9239	10.1831	.7796	-1.9876	-10.5810	-10.1635
11	.7195	62.1793	8.5027	-.3419	.2067	6.0066	6.3548	8.9972	5.5078	8.2876	-16.9167	-.8170
12	.5892	62.6965	8.0768	-.3221	.1538	6.8003	7.2552	5.2219	7.4677	14.3385	-15.8717	9.7275
13	.5281	63.1683	7.8447	-.3105	.1222	7.2269	7.7657	1.9891	7.8214	16.6367	-7.0466	15.3331
14	.4923	63.6386	7.3688	-.2895	.1069	7.1392	7.7375	-2.5584	4.6029	11.1930	5.3483	11.4733
15	.4738	64.1155	6.4683	-.2522	.0888	6.3989	6.9916	-8.9646	.3319	.8658	21.4909	.8658
16	.4576	64.6138	4.7011	-.1819	.0624	4.7399	5.2221	-19.2833	-.8816	-2.4188	48.0817	-2.4188
17	.4523	65.1310	1.9101	-.0733	.0253	1.9414	2.1600	-20.0388	.2036	.4389	50.5751	8.5058
18	.5078	65.6053	.2511	-.0096	.0033	.2825	.3167	-6.7123	1.0536	3.2203	14.0011	9.3066
19	.6556	66.0230	.1472	-.0056	.0019	.1809	.2037	1.6353	-1.2908	-4.0330	-.9654	-4.7641
20	.8520	66.4039	.6182	-.0233	.0080	.3917	.4433	-------	------	-------	-------	-------
21	1.0937	66.7634	1.0389	-.0389	.0118	.4602	.5242	-------	------	-------	-------	-------
22	1.3390	67.1491	------	------	-------	------	------	-------	------	-------	-------	-------
23	1.5919	67.5569	------	------	-------	------	------	-------	------	-------	-------	-------

TABLE II - MASS-FLOW VARIATION AT STATION 12

NACA

φ	① $W_{1,m}^*$	② $\left(\frac{\partial W_1^*}{\partial \varphi}\right)_m$	③ $\left(\frac{\partial^2 W_1^*}{\partial \varphi^2}\right)_m$	④ $\varphi-\varphi_m$	⑤ $\frac{1}{2}$ ④ ^{2}	⑥ W_1^* ①+②④+③⑤	⑦ $W_{\varphi,m}^*$	⑧ $\left(\frac{\partial W_\varphi^*}{\partial \varphi}\right)_m$	⑨ $\left(\frac{\partial^2 W_\varphi^*}{\partial \varphi^2}\right)_m$	⑩ W_φ^* ⑦+④⑧+⑤⑨	⑪ W^{*2} ⑥^2+⑩^2	⑫ $\frac{I^*+\frac{1}{2}U_1^{*2}r^{*2}-\frac{1}{2}W^{*2}}{hf}$ 1.0632 − 0.0084×⑪	⑬ ρ^* ⑫ 2.5	⑭ $r^*r^*\rho^*W_1^*$ 0.9571 ⑬⑥	⑮ M	⑯ Total mass flow	⑰ Percentage mass flow
-0.8152	------	------	------	-0.2169	0.023550	-0.2882	------	------	-------	-0.8065	0.1256	1.0621	1.1628	-0.3140	0.0779	------	--
-.7610	------	------	------	-.1627	.013235	-.0016	------	------	-------	-.1781	.0321	1.0629	1.1847	-.0017	.0866	------	24
-.7068	------	------	------	-.1086	.005882	.3137	------	------	-------	-.1927	.1358	1.0621	1.1838	.3418	.0775	------	--
-.6525	------	------	------	-.0542	.001471	.6578	------	------	-------	-.2472	.4935	1.0591	1.1844	.7114	------	------	--
-.5983	1.0301	7.1321	9.7275	0	0	1.0301	-0.3424	-2.1321	-13.8717	-.3424	1.1763	1.0535	1.1388	1.0991	------	0.3654	--
-.5448	------	------	------	.0535	.001431	1.4256	------	------	-------	-.4764	2.2595	1.0442	1.1142	1.4885	------	------	--
-.4913	------	------	------	.1070	.005724	1.8489	------	------	-------	-.6499	3.8408	1.0309	1.0790	1.8698	.1691	------	--
-.4378	------	------	------	.1606	.012880	2.3001	------	------	-------	-.8633	6.0357	1.0125	1.0315	2.2233	.2688	------	76
-.3843	------	------	------	.2140	.022898	2.7781	------	------	-------	-1.1163	8.9695	.9879	.9700	2.6262	.3861	------	--

TABLE III - RESIDUALS OBTAINED IN CENTRIFUGAL IMPELLER

φ	Station										
	7	8	9	10	11	12	13	14	15	16	17
-0.80	------	------	------	------	------	------	------	------	------	------	------
-.75	------	------	------	------	------	0.3208	-0.5986	-0.3198	-0.2762	-1.8827	-0.9203
-.70	------	------	------	------	------	.0531	-.0132	-.6849	.4481	-1.4503	-.2995
-.65	------	------	------	-0.4237	-0.0496	.0583	-.3224	-.1166	.0428	-.6472	-.2425
-.60	------	------	------	-.4498	.1272	-.1133	-.5021	.0383	-.3632	-.1410	-.2351
-.55	------	------	0.3820	-.6658	.0875	-.1688	.0710	.1207	.0544	-.3666	.0225
-.50	------	-0.1122	-.4411	.6046	-.9682	.2019	.2963	-.7490	-.0897	-.0897	-.3331
-.45	------	-.7145	.3554	-.2592	-.0411	-.0177	------	------	------	------	------
-.40	------	.4582	-.2200	.2748	------	------	------	------	------	------	------
-.35	-0.1596	.0332	.4425	------	------	------	------	------	------	------	------
-.30	-2.6699	-.7140	------	------	------	------	------	------	------	------	------
-.25	-2.8672	.5540	------	------	------	------	------	------	------	------	------
-.20	-2.0695	------	------	------	------	------	------	------	------	------	------
-.15	-1.7244	------	------	------	------	------	------	------	------	------	------
-.10	------	------	------	------	------	------	------	------	------	------	------

TABLE IV - ESTIMATED PERCENTAGE ERROR IN $\rho^* W_i^*$

φ	Station										
	7	8	9	10	11	12	13	14	15	16	17
-0.75	------	------	------	------	------	0.1001	-0.3010	0.2672	-0.4396	-0.2266	-0.1695
-.70	------	------	------	------	------	.0176	-.0198	-.0159	-.0270	-.1279	-.0469
-.65	------	------	------	-0.0091	-0.0276	.0074	.0226	.0358	.0435	-.0780	-.0036
-.60	------	------	------	.0095	-.0048	.0075	-.0132	-.0083	-.0004	-.0120	-.0123
-.55	------	------	0.1067	-.0304	.0292	-.0082	-.0209	.0212	-.0128	-.0017	.0039
-.50	------	0.0907	.0007	-.0094	.0028	-.0032	-.0022	.0578	.0085	-.0293	.0474
-.45	------	-.0138	-.0048	.0065	-.0695	.0187	------	------	------	------	------
-.40	------	-.0155	-.0017	-.0431	------	------	------	------	------	------	------
-.35	0.0615	.0219	-.0451	------	------	------	------	------	------	------	------
-.30	-.0240	-.0091	------	------	------	------	------	------	------	------	------
-.25	-.0107	-.0769	------	------	------	------	------	------	------	------	------
-.20	-.0204	------	------	------	------	------	------	------	------	------	------
-.15	-.0437	------	------	------	------	------	------	------	------	------	------

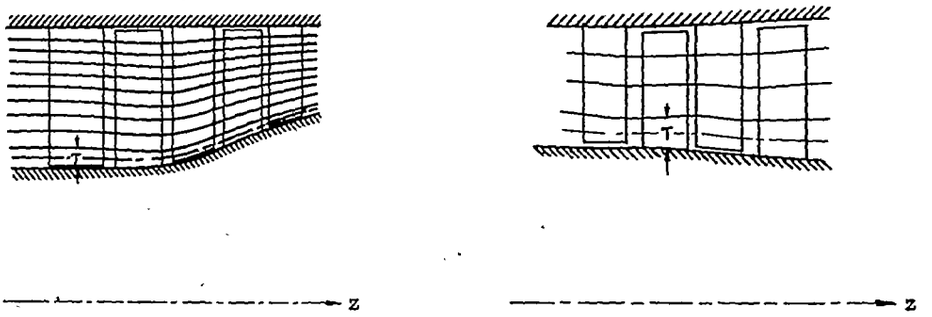

(a) Axial-flow compressor. (b) Axial-flow turbine.

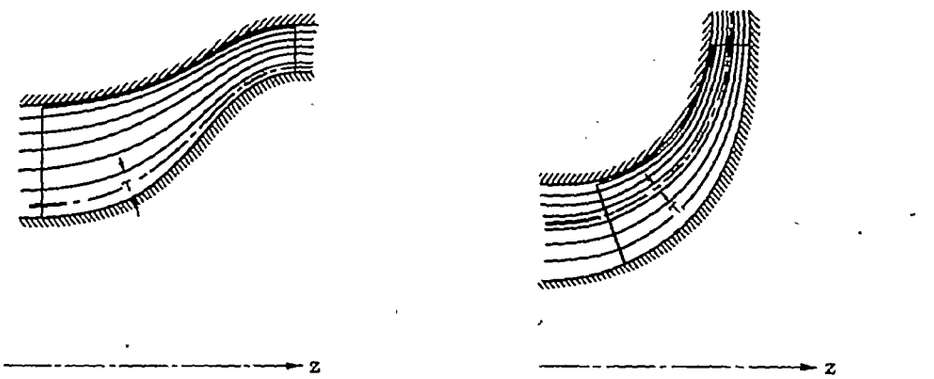

(c) Mixed-flow compressor. (d) Centrifugal compressor.

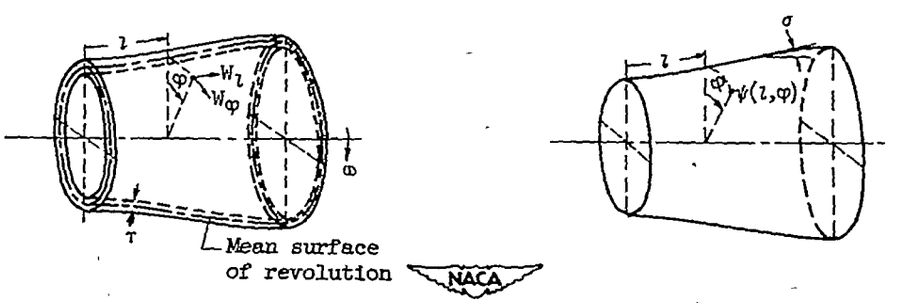

(e) Mean surface of revolution and orthogonal coordinates l and φ on it.

Figure 1. - Flow along stream filaments of revolution in various types of turbomachine and orthogonal coordinates for mean stream surface of revolution.

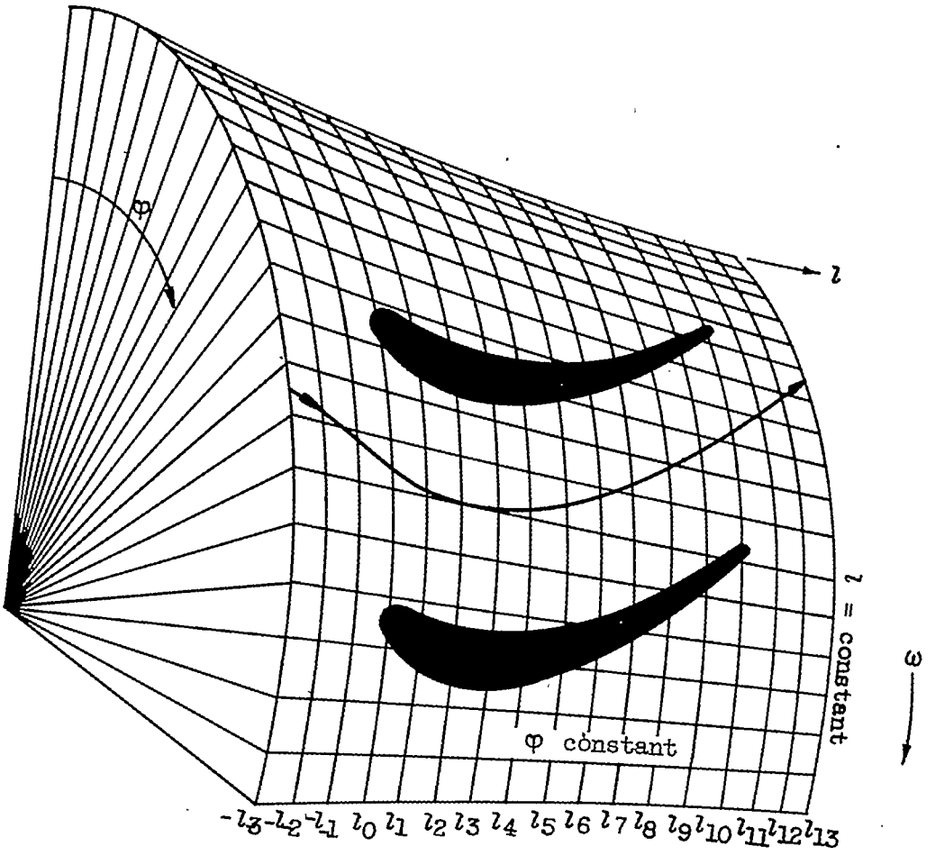

(a) Gas turbine.

Figure 2. - Blade sections on mean surface of revolution.

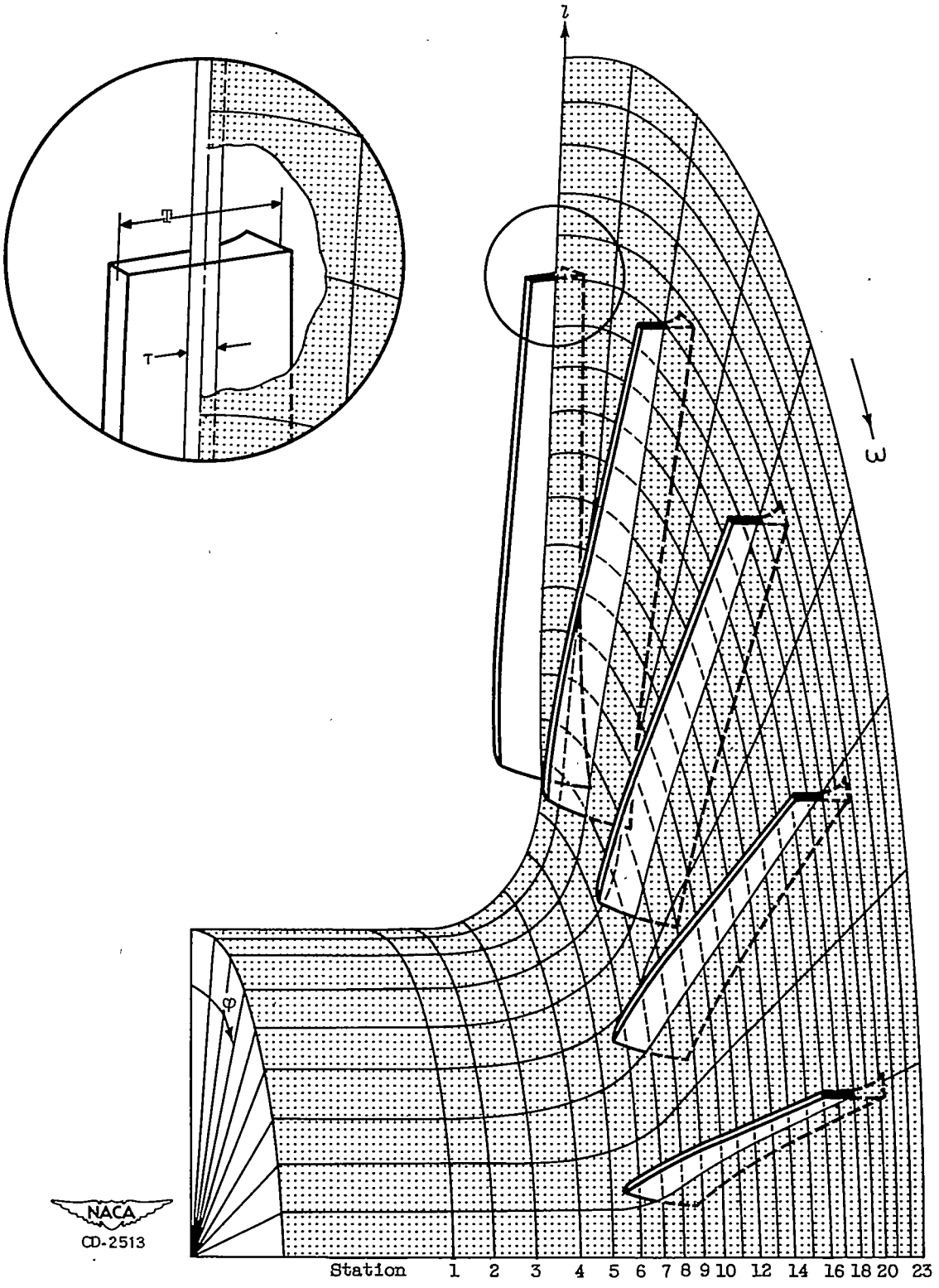

(b) Centrifugal compressor

Figure 2. - Concluded. Blade sections on mean surface of revolution.

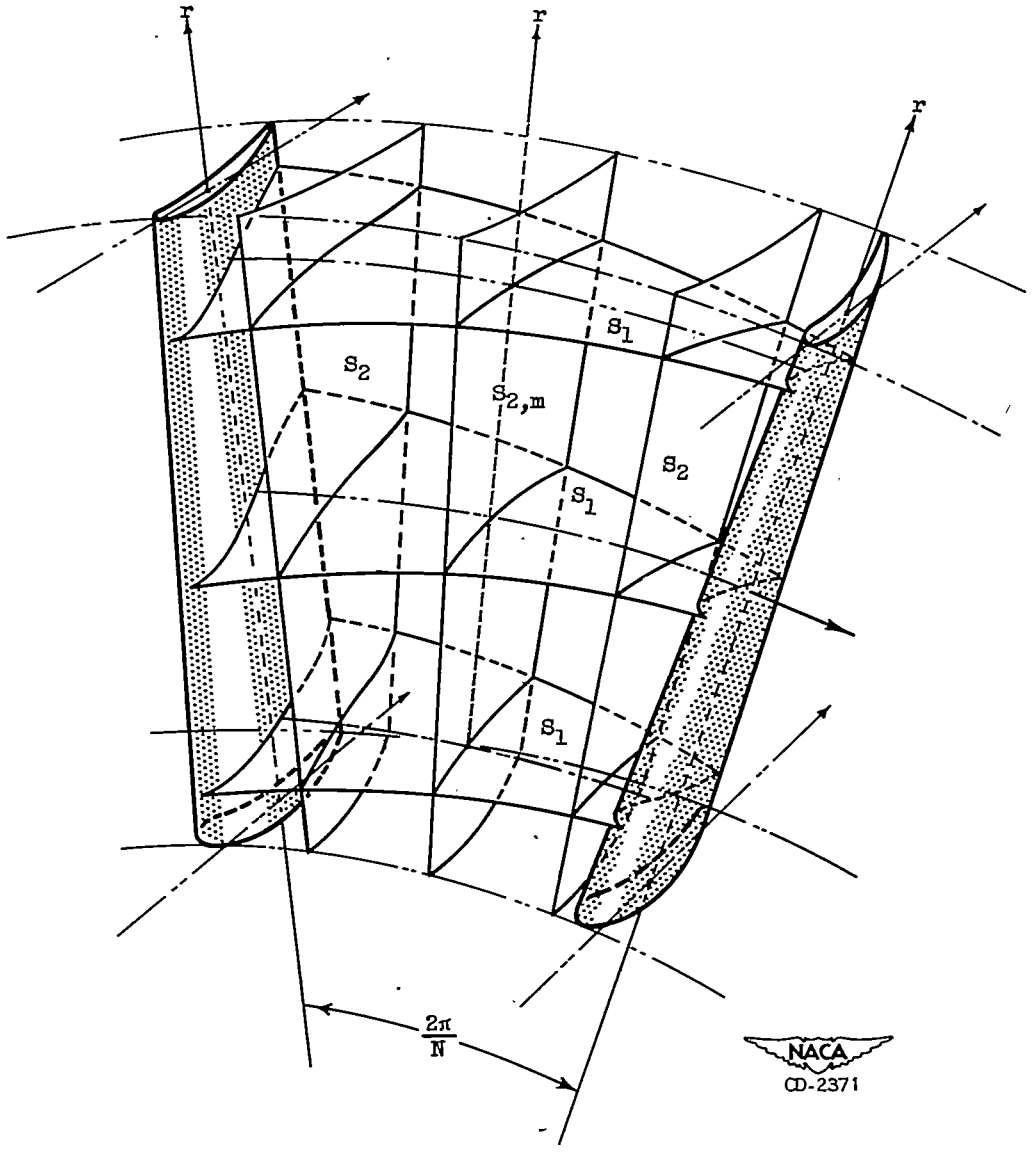

Figure 3. - Intersecting S_1 and S_2 surfaces in a blade row.

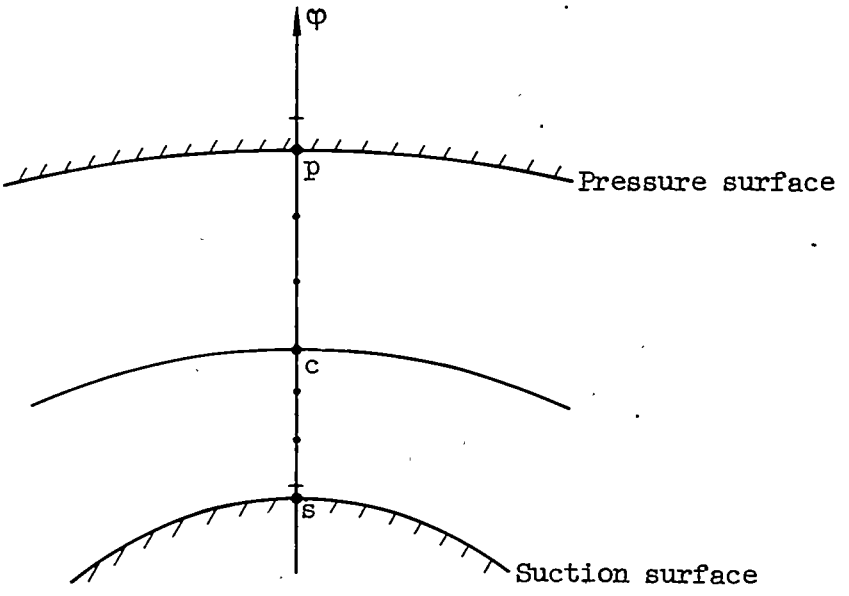

(a) Stations along φ.

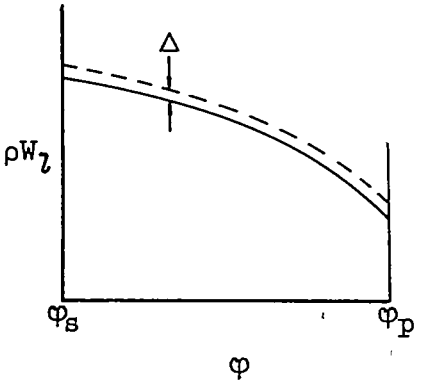

(b) Variation of ρW_l and its correction across channel.

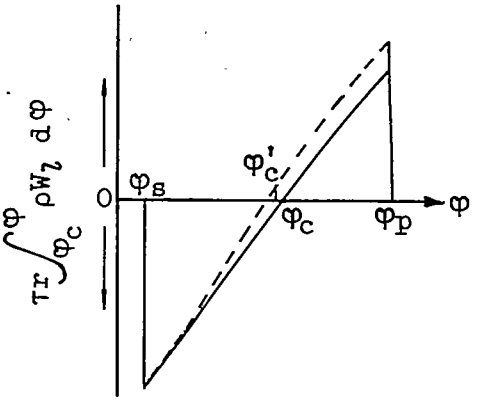

(c) Mass flow across channel and its correction.

Figure 4. - Corrections for position of chosen streamline and specific mass flow across channel.

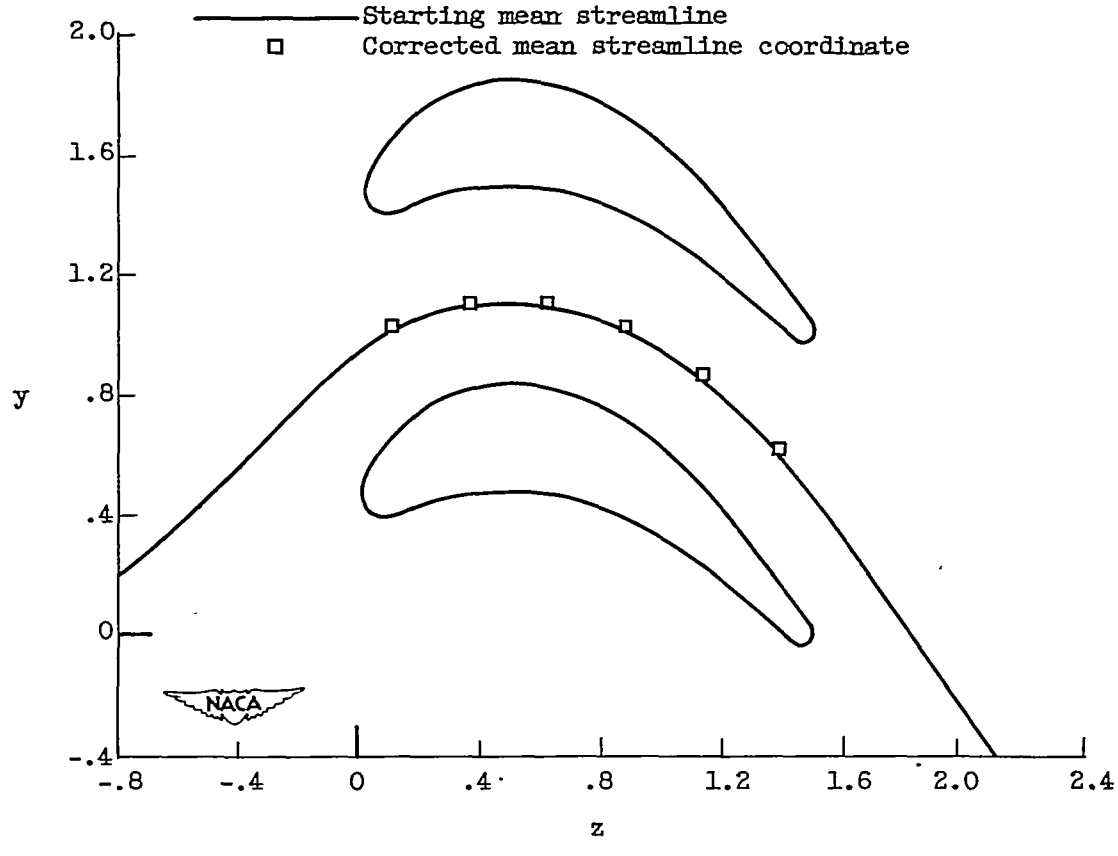

(a) Mean streamline.

Figure 5. - Starting and corrected values for turbine cascade.

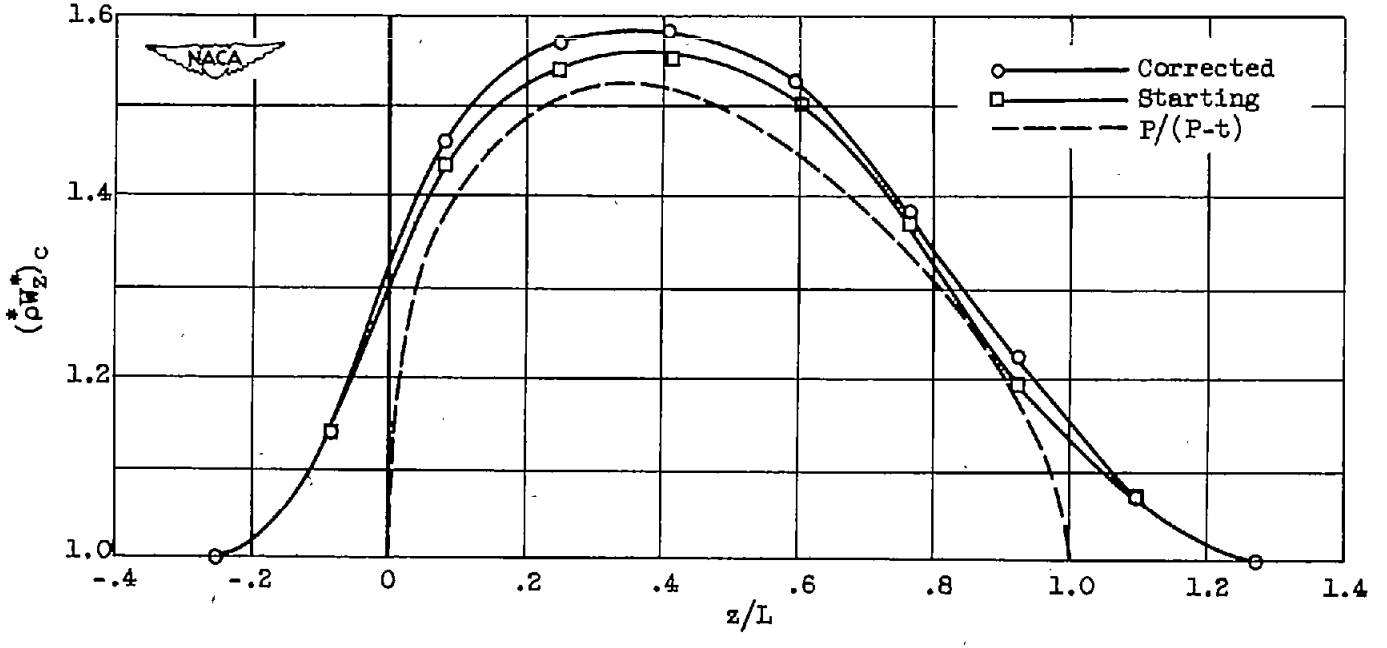

(b) $(\overset{*}{\rho}W_z^*)_c$ plotted against z/L.

Figure 5. - Concluded. Starting and corrected values for turbine cascade.

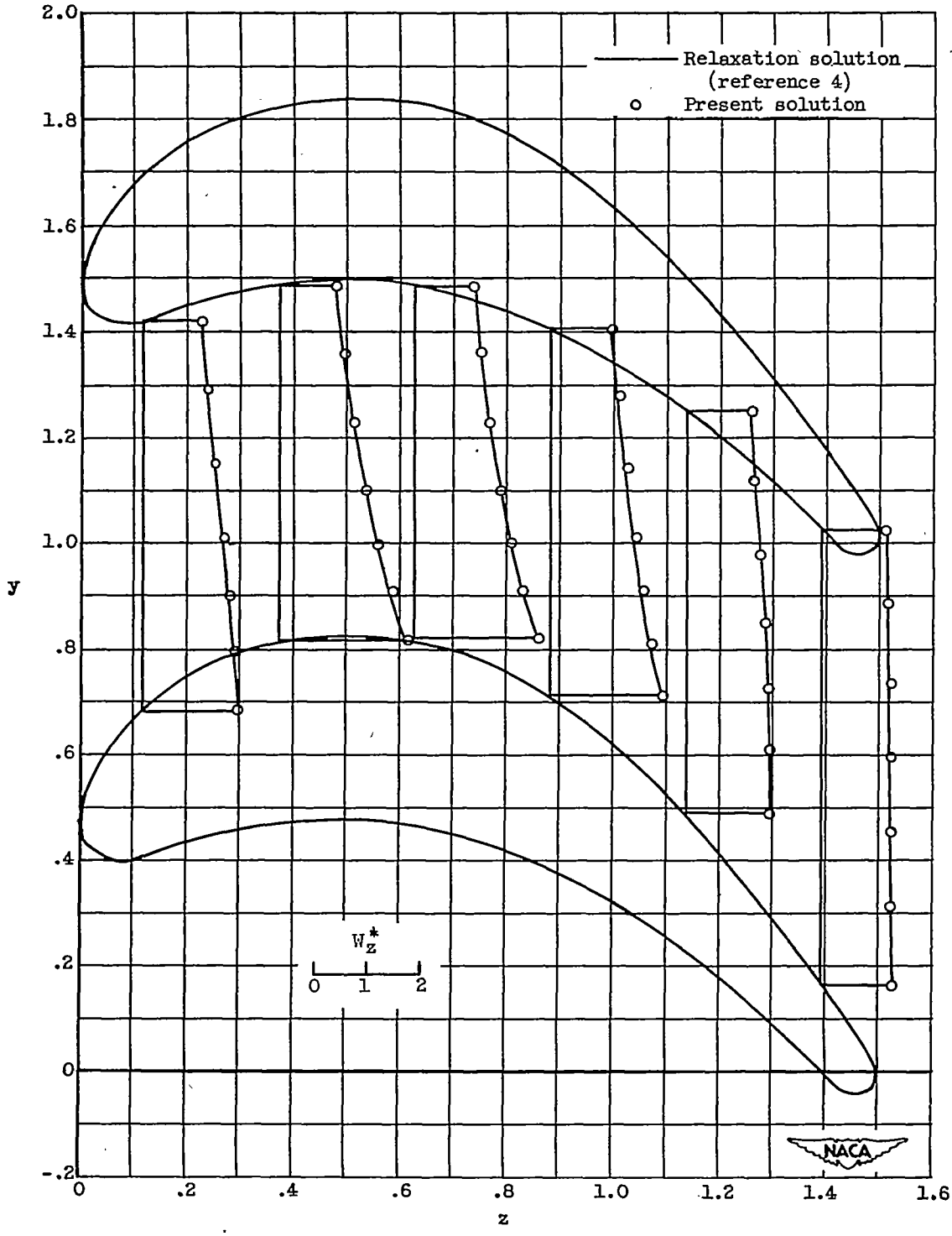

(a) Axial component.

Figure 6. - Comparison of velocities for present and relaxation solutions for turbine cascade.

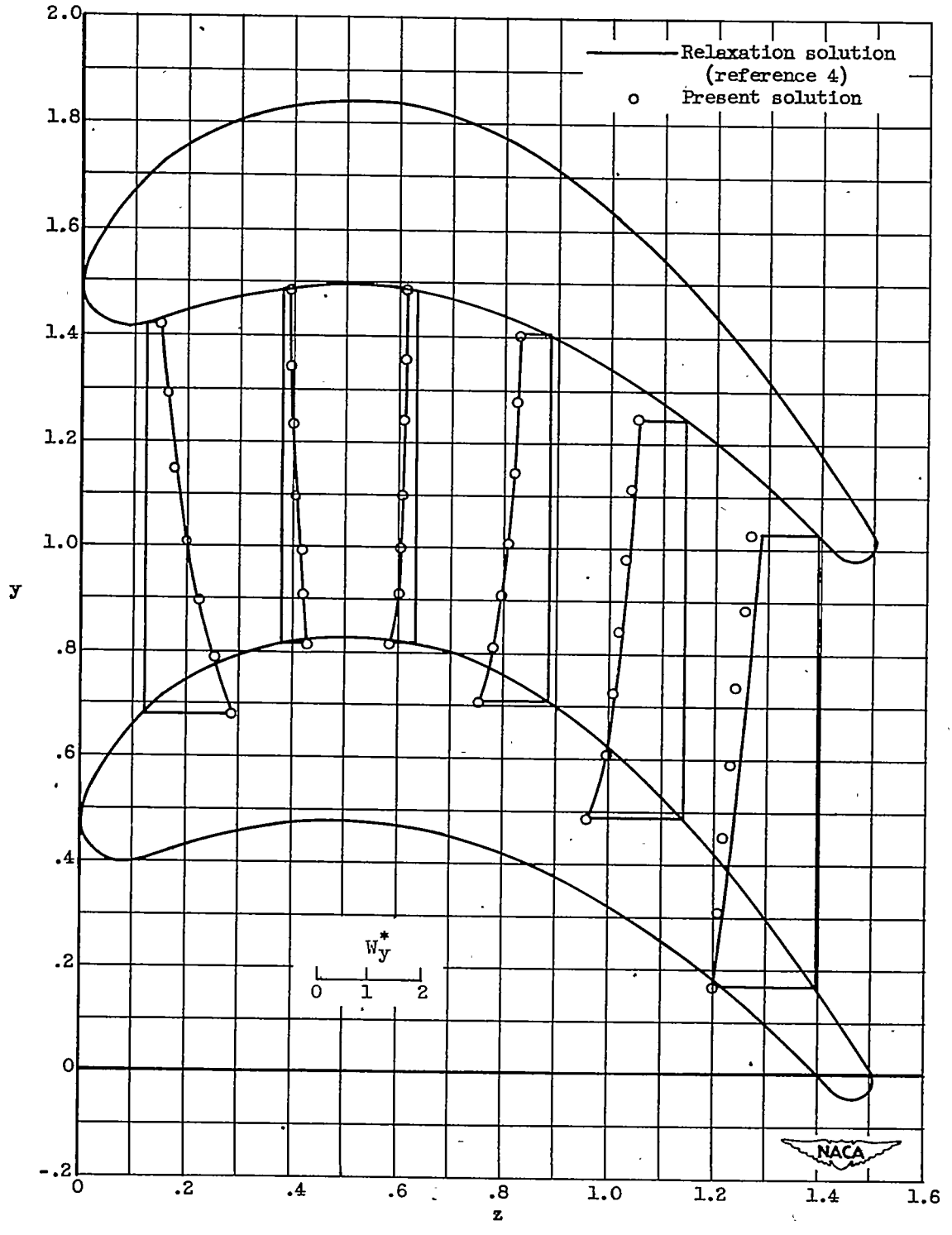

(b) Tangential component.

Figure 6. - Continued. Comparison of velocities for present and relaxation solutions for turbine cascade.

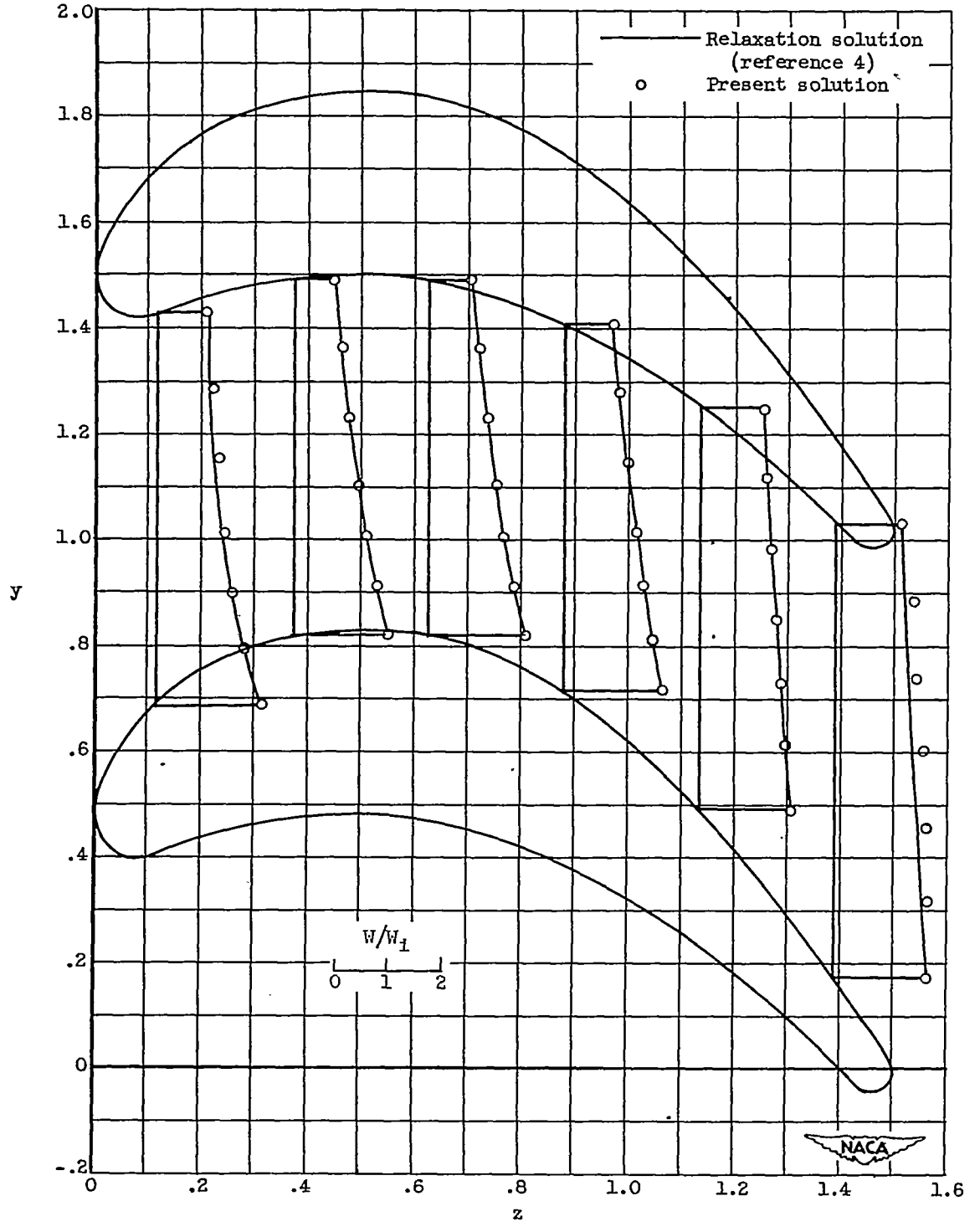

(c) Resultant.

Figure 6. - Concluded. Comparison of velocities for present and relaxation solutions for turbine cascade.

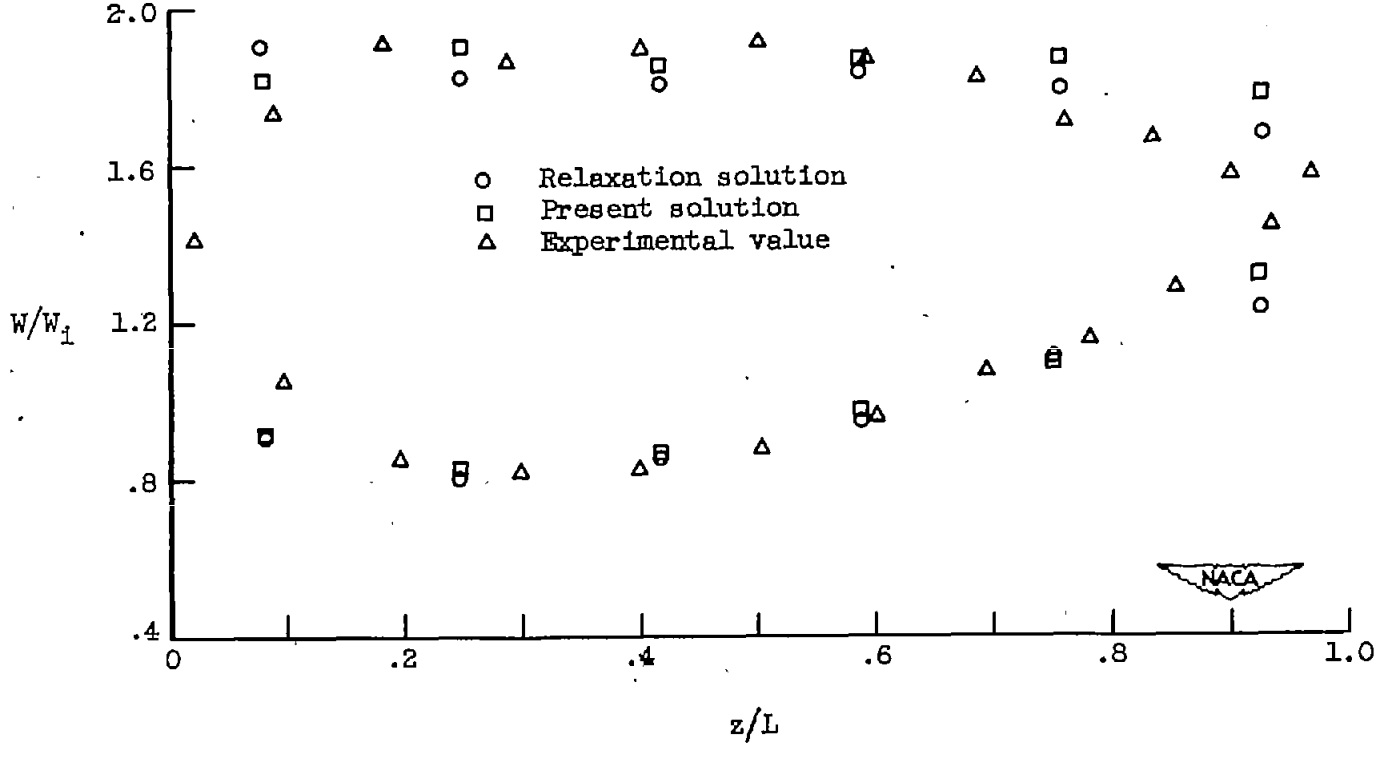

Figure 7. - Comparison of velocity distribution around blade surface obtained in present solution with relaxation solution and experimental value of reference 1.

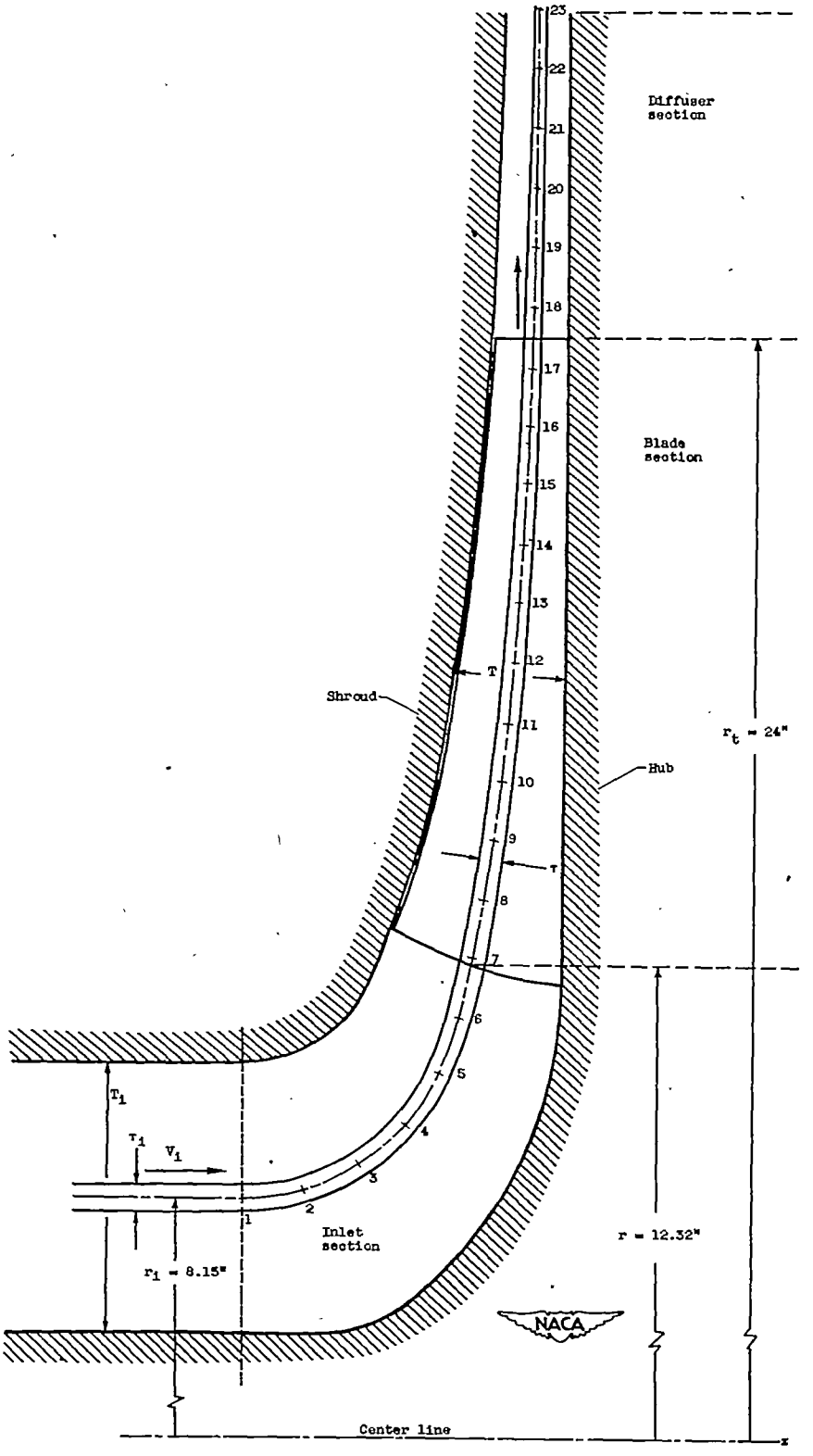

Figure 8. - Meridian section of impeller and geometric mean stream surface.

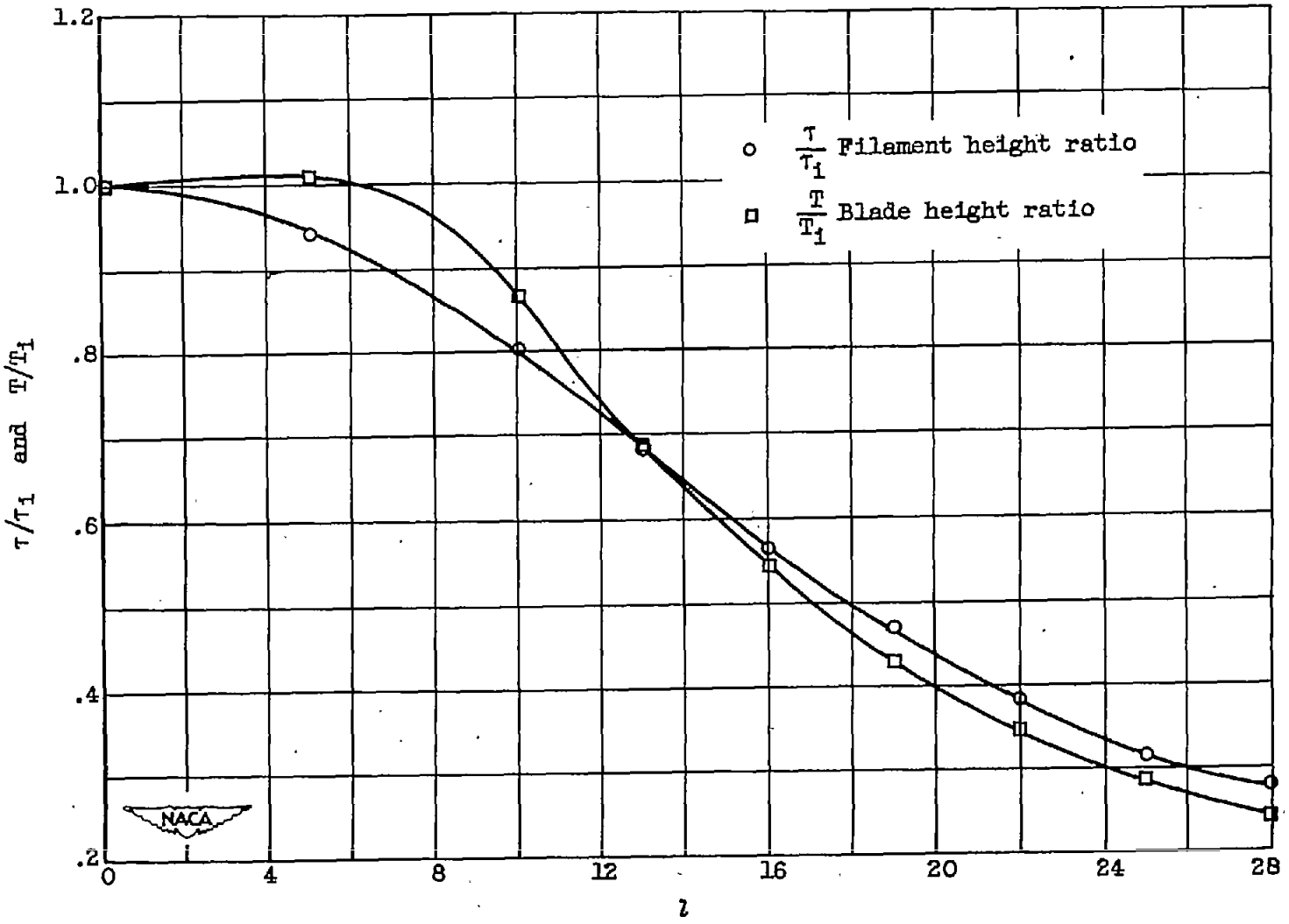

Figure 9. - Variation of normal thickness of stream filament of revolution and normal height of impeller blade in meridional plane for centrifugal impeller.

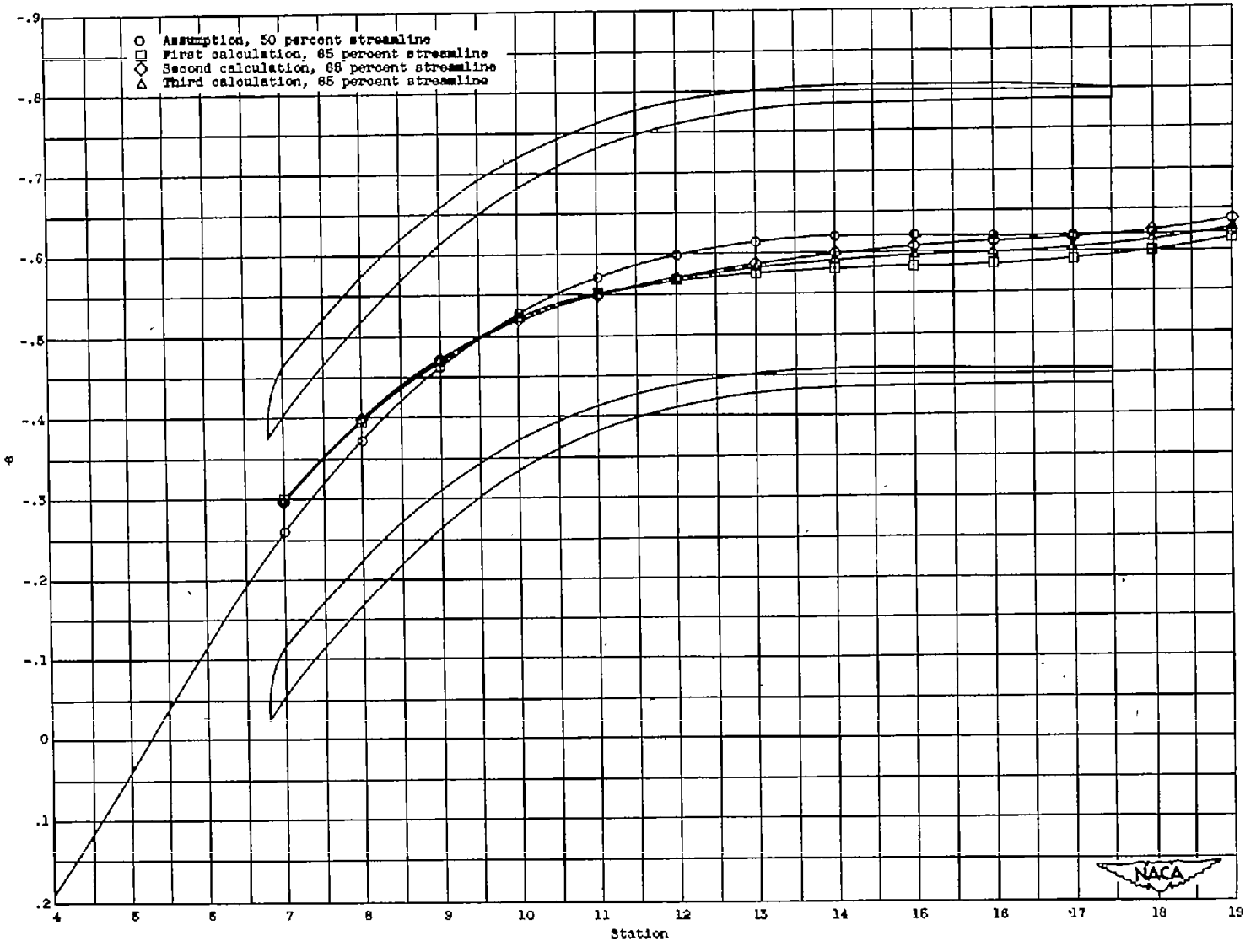

Figure 10. - Chosen streamlines in passage for different computing cycles for centrifugal impeller.

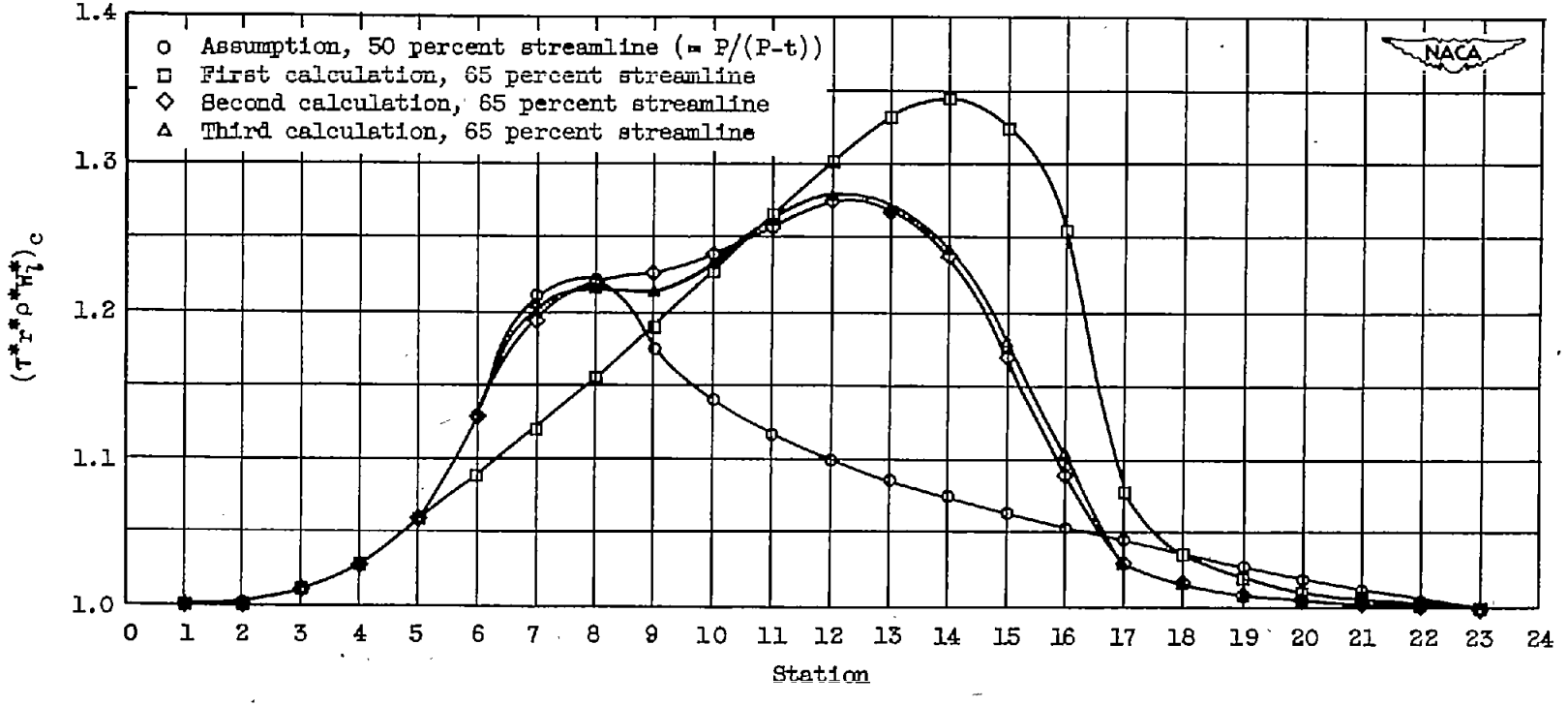

(a) $(\tau^* r^* \rho^* W_l^*)_c$ for various stations.

Figure 11. - Variations on chosen streamline for progressive cycles of computation for centrifugal impeller.

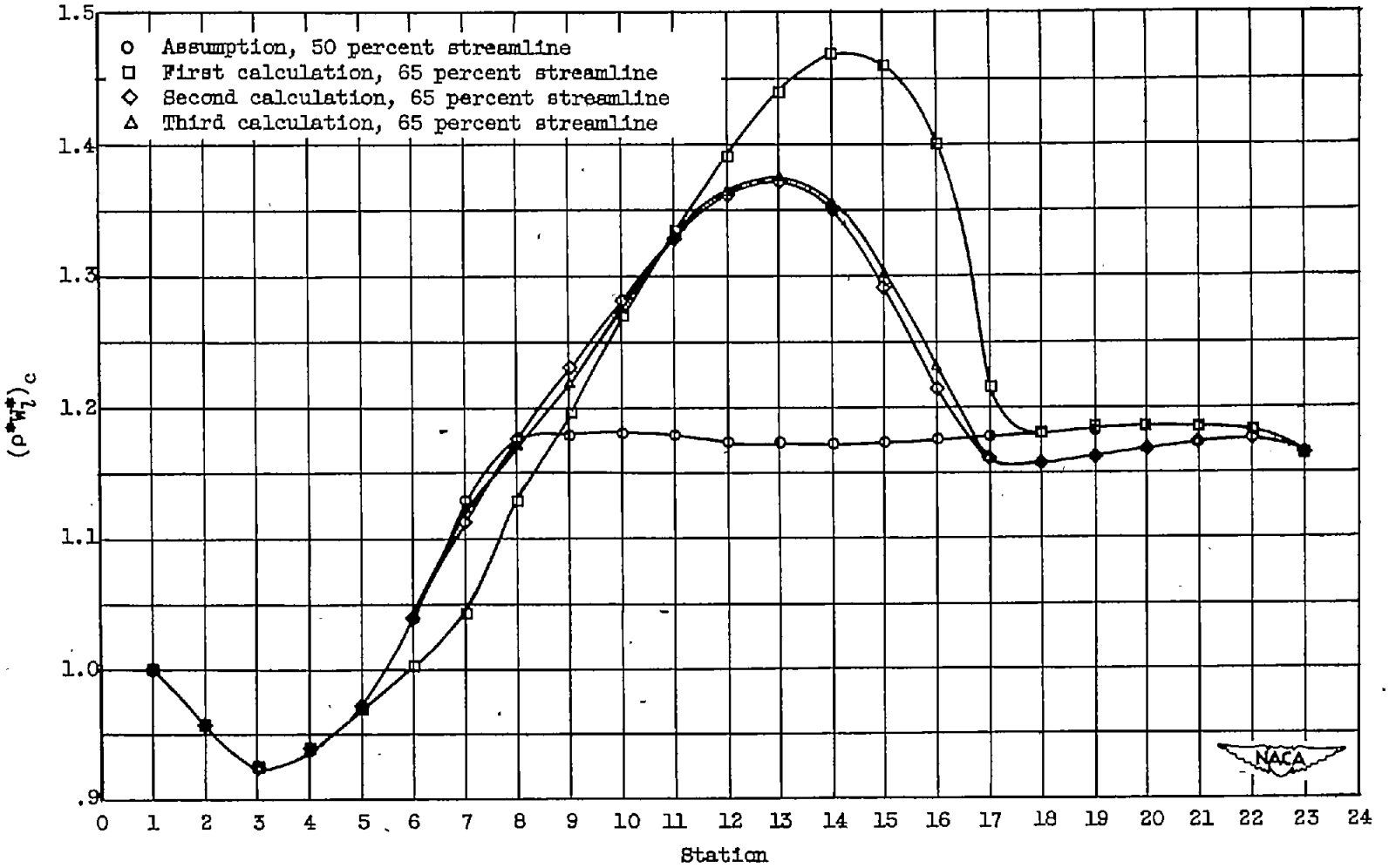

(b) $(\rho^* W_l^*)_c$ for various stations.

Figure 11. - Concluded. Variations on chosen streamline for progressive cycles of computation for centrifugal impeller.

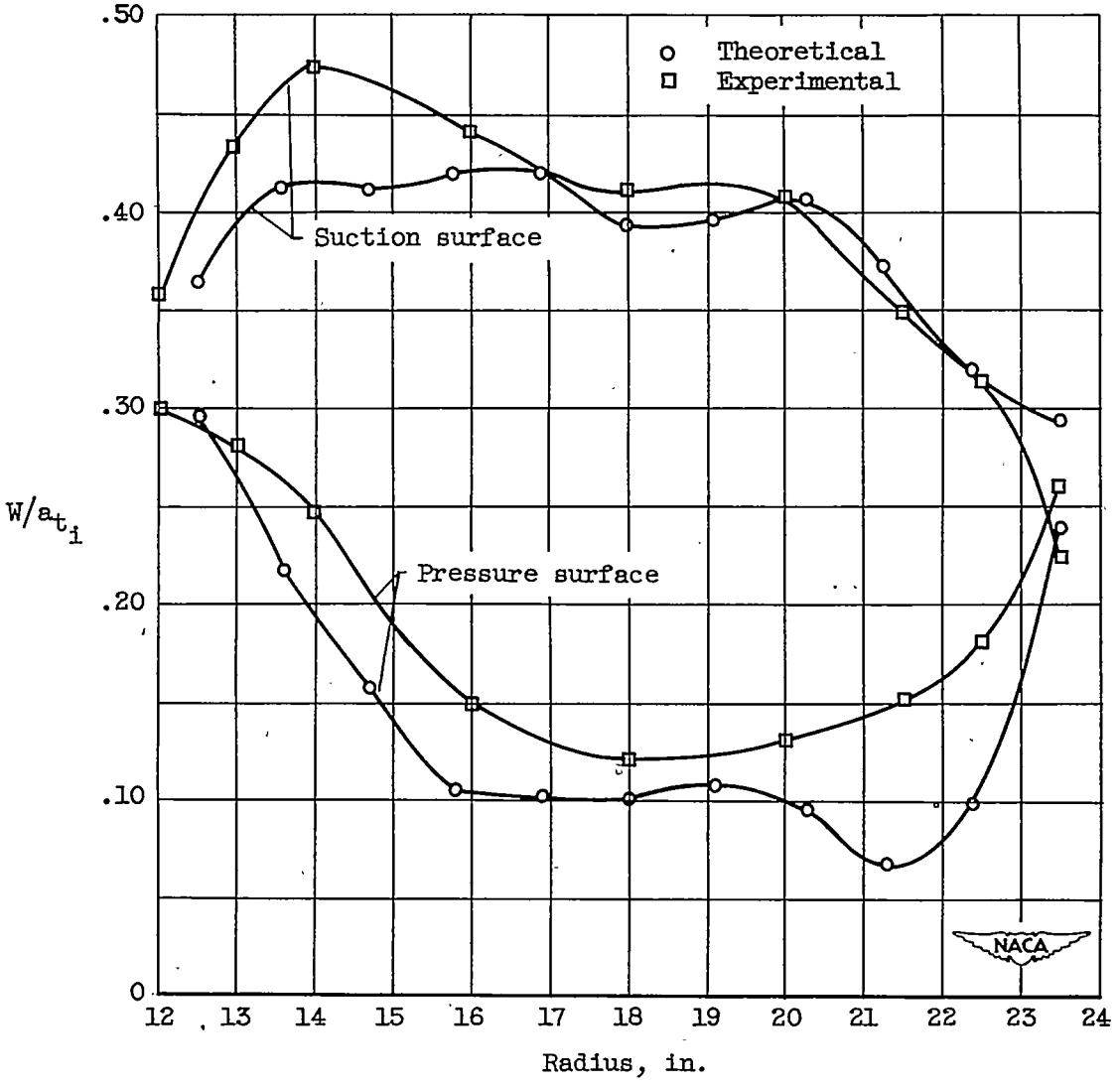

Figure 12. - Theoretical and experimental velocity distribution near blade surfaces for centrifugal impeller.

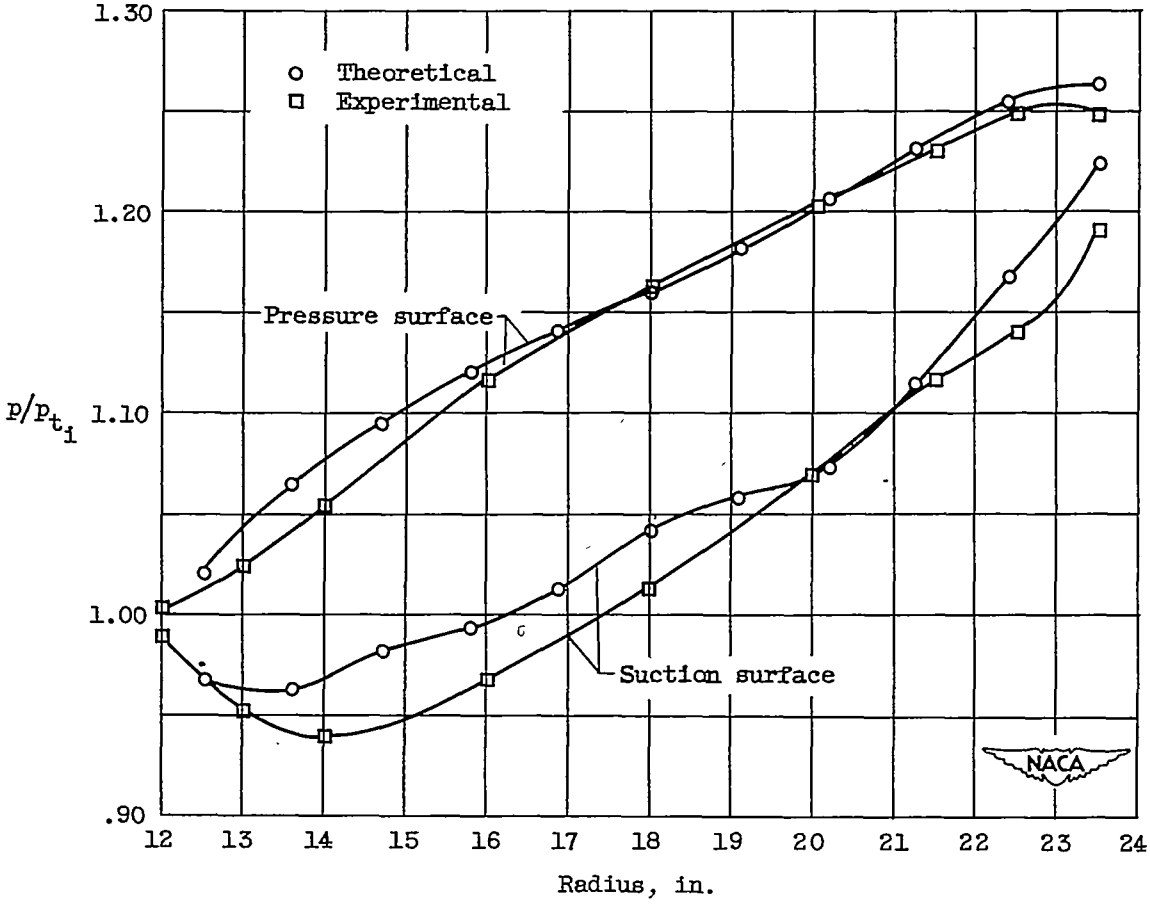

Figure 13. - Theoretical and experimental static-pressure distribution along blade surfaces for centrifugal impeller.

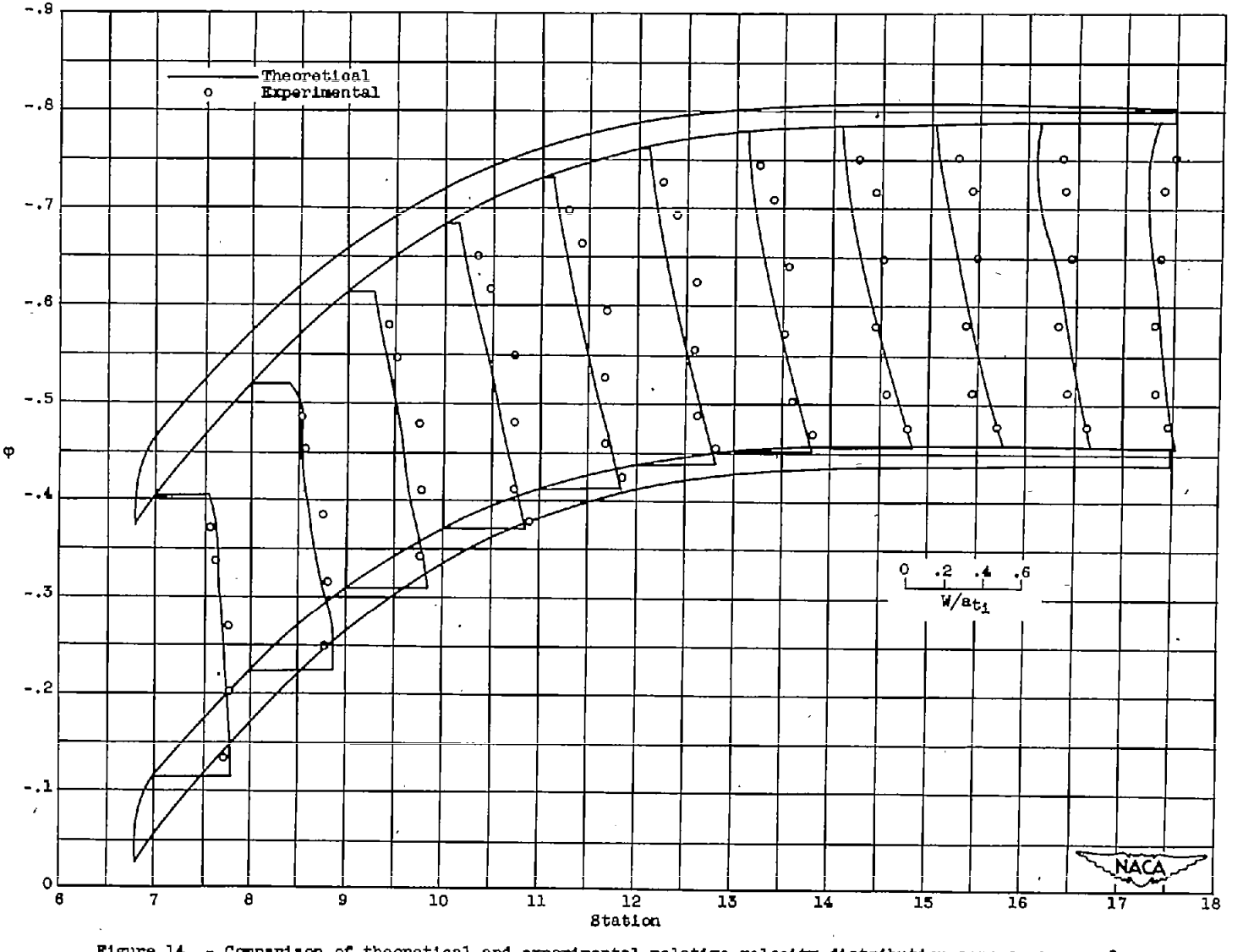

Figure 14. - Comparison of theoretical and experimental relative velocity distribution across passage for centrifugal impeller.

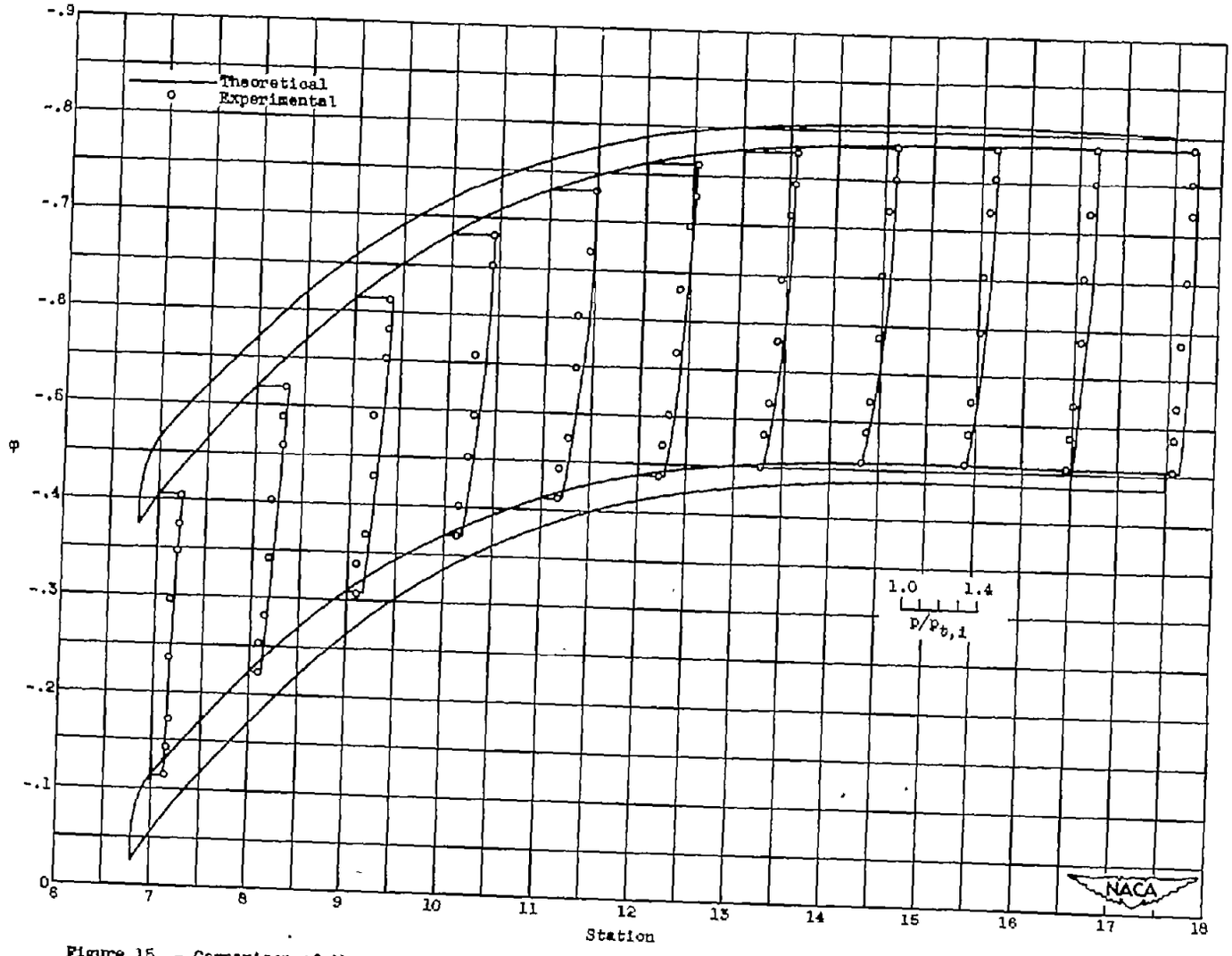

Figure 15. - Comparison of theoretical and experimental static-pressure distribution across passage for centrifugal impeller. Pressure-ratio reference line is at 1.0.

NACA-Langley - 8-10-53 - 1000